Universidad Rey Juan Carlos

BACHELOR IN AEROSPACE ENGINEERING

BACHELOR THESIS

Generalized Logarithmic Spirals for the Preliminary Design of Low-Thrust Trajectories to the Asteroid Belt

Author:
Alejandro de Miguel Mendiola

Supervisor:
Dr. Hodei Urrutxua Cereijo

July 31, 2018

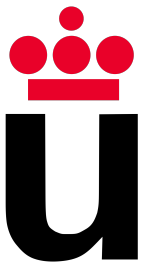

To confine our attention to terrestrial matters
would be to limit the human spirit.
-Stephen Hawking

Abstract

THE design of low-thrust spacecraft trajectories naturally leads to solving an Optimal Control Problem (OCP). This is customarily solved using a direct transcription method, which requires an initial guess for the low-thrust trajectory in order to initialise the numerical solver. The initial guess is of paramount importance, since a bad guess might prevent the solver from converging. Therefore, many studies have sought for geometric constructions of approximate spiralling trajectories, which closely match the thrust profiles of low-thrust trajectories, thus providing reasonable initial guesses for solving the OCP. One such class of spiralling trajectories is the recently proposed class of Generalised Logarithmic Spirals (GLS), which has proven to be extremely versatile, not only offering very compelling initial guesses for OCPs, but also providing straightaway multiple transfer options which are useful for preliminary mission analysis purposes. Thus, the use of GLS for trajectory design has rapidly gained popularity and become a powerful technique for the design of low-thrust trajectories. This Engineering Thesis will look into applications of GLS for the design of low-thrust orbital transfers from the Earth to asteroid belt objects, and among asteroids within the belt.

Resumen

El diseño de trayectorias de bajo empuje, por su naturaleza, conlleva resolver un problema de control óptimo (*Optimal Control Problem*, OCP). Normalmente estos problemas son resueltos usando un método de transcripción directa, el cual requiere una estimación inicial de la posible solución de la trayectoria, para inicializar dicho método numérico. Esta estimación inicial es increíblemente importante, ya que una mala estimación puede evitar la convergencia del método hacia la solución. Por tanto, numerosos estudios se han dedicado a encontrar construcciones geométricas de trayectorias espirales aproximadas que representen fielmente los perfiles de empuje de las trayectorias de bajo empuje, obteniendo así buenas estimaciones iniciales para los métodos numéricos destinados a resolver el problema de control óptimo. Uno de estos estudios sobre trayectorias espirales es el presentado en esta tésis, las espirales logarítmicas generalizadas (*Generalized Logarithmic Spirals*,GLS). Este método ha probado ser extremamente versátil, ya que no sólo ofrece estimaciones iniciales competentes para los problemas de control óptimo, sino que también ofrece múltiples soluciones de transferencias orbitales, muy útiles para el análisis preliminar de misiones. Debido a sus múltiples ventajas, el uso de las espirales logarítmicas generalizadas ha crecido rápidamente en popularidad, llegándose a convertir en una herramienta muy potente para el diseño de trayectorias de bajo empuje. Esta tésis de ingeniería tiene como objetivo aplicar el método de las espirales logarítmicas generalizadas para el diseño de transferencias orbitales de bajo empuje desde la Tierra hasta el cinturón de asteroides.

Acknowledgments

Gracias, to all my family, for your love and your encouragement in all the decisions I have made to this moment. With this thesis I would like to pay you back, at least a little bit, all the sacrifices you have made to allow me to get this far, and to thank you for supporting me no matter what.

Gracias, Pablo Castell , for sharing with me days, laughs, goals and dreams.

Gracias, Pedro Arias, for your words of wisdom and for your unconditional trust.

Gracias, Lucía Acevedo, for your strong support in the bad times and the wonderful moments you have given me.

Gracias, Carlos Rámila, Julia Oviedo, Manuel Contin, for your long-lasting friendship.

Gracias, classmates, for sharing these special years of my life. Specially to Borja, Carmen and Paula who most closely travelled with me these years, and luckily the next ones.

Gracias, Hodei, for the idea and opportunity of working in this thesis. The little I know about astrodynamics is because of you. But mostly, thank you for your time, endless patience and for your always open door at your office.

Gracias, finally, to all the people, friends and teachers, I have encountered until this moment. It is impossible to name you all, but I thank you for stepping into my life because a little bit of each of you is what has made me who I am.

Contents

Chapter 1

Introduction

"The more I learn, the more I realize how much I don't know."
-Alber Einstein

HISTORICALLY, space exploration has been carried out since ancient civilizations. It is true that physical space exploration had not been achieved until the mid-twentieth century, when technology developed enough to put people in space thanks to rockets and space stations. However, the observation of objects in space, in other words, astronomy, dates back to civilizations such as Babylonians, Greeks, Indians, Egyptians, Iranians, Chinese and Maya.

Human race has been always connected and attracted by space. We have looked up into it when we needed answers, but most importantly when we needed something to believe in, to hold to. Greeks and Romans found their Gods in planets; shooting stars provide wishes to anyone lucky enough to contemplate one; aliens have inspired many tales, books and movies; stars have guided those who were lost. Ironically, space, although empty as it is, has filled our hearts and keeps quenching the thirst for knowledge of our kind.

Nowadays, some may say space exploration is a waste of money, that there is no need for going so far away just to study a rock, that Earth problems should be fixed before we even consider to fix others. But space makes us progress, it brings out our best, it unites us as a species.

All of it to be better, all of it to get further, all of it to dream longer.

1.1 Motivation

This thesis has been inspired by the possibilities space exploration holds. More specifically, asteroid exploration. Why observe and study them? Why go there? Why asteroids?

Asteroids are part or the early solar system's history. It is believed that asteroids formed about 4.5 billion years ago due to the collapse of a cloud of hydrogen gas and interstellar dust that also formed the planets and the Sun. Therefore, understanding the formation of asteroids is, in a way, equivalent to understanding the formation of our solar system, which is fundamental in order to answer the most compelling questions of human kind.

Not only that, asteroids are one of the most valuable resources in space.

Asteroid mining is the exploitation of raw materials from asteroids. These materials can be used for space constructions or to take them back to Earth. The materials that could be obtained from an asteroid are really diverse, for example: iron, aluminum, titanium, nickel for construction; or gold, silver, iridium, platinum and tungsten for Earth import.

The fact that material could be exploited directly in space would facilitate the concept of space construction because materials, or even the machines required for construction, would not need to be transported from the Earth.

Also, spacecraft propellant could also be processed from the asteroid's resources, making in-space propellant supply a reality (which would increase the possibilities and range of space missions). Ice, present in a lot of asteroids and comets, could provide water, enabling human expansion into the solar system.

Lastly, these asteroid mining missions could be very profitable, because of the precious stones and rare Earth materials that can be obtained from asteroids.

The knowledge, the resources and the possibilities asteroid mining and research gives, are more than enough to justify the questions above. The time is now, future begins here.

1.2 Historical Perspective

NEAR Shoemaker (Near Earth Asteroid Rendezvous) was the first spacecraft to orbit, land on and send data from the surface of an asteroid. It was launched on February 17, 1996 and it succeeded on February 12, 2001, when it touched down the asteroid. The main goal of the mission was to study the second largest near Earth asteroid, Eros, from its orbit, for over a

year. It gathered data from the asteroid's properties such as shape, rotation and composition.[1]

After this first mission to explore asteroids there were others, but one of the most ambitious was the mission Dawn. Dawn was a NASA mission that aimed to explore two of the oldest and most massive asteroids in the asteroids belt: Vesta and Ceres. Launched on September, 2007, the mission should have ended on June, 2016, after orbiting Vesta for over a year and arriving at Ceres. But NASA has extended the mission until the fuel runs out. The mission is still operative. Currently, on July, 2018, Dawn is in its elliptical orbit, transmitting all its findings to Earth.[2]

OSIRIS-REx may be considered the pioneer in asteroid mining. The mission was launched on September, 2016 and it is headed to the asteroid Bennu, a near-Earth asteroid classified as a potentially hazardous object due to the possibility to impact the Earth late in the twenty-second century. The mission will study the asteroid to investigate how planets formed, and also it will determine Bennu's physical and chemical properties, which would help scientist in a possible future impact mitigation mission. But the other main goal of the mission is to return a sample, of at least 60 grams up to 2 kilograms, back to Earth. The mission is still in progress, approach will begin on August 2018 and is expected to arrive at Bennu on December, 2018. The sample will be acquired on July, 2020 thanks to a robotic arm. The return to Earth phase will take place on March, 2021, to finally arrive to Earth on September, 2023, concluding the seven year journey of the mission. [3]

As in the future (launch is scheduled on October, 2021), Lucy will be the first mission to visit Jupiter's Trojans, a swarm of asteroids that are thought to be remnants of the primordial material that formed the outer planets. These asteroids orbit the Sun in two groups, one ahead of Jupiter (called Greek camp) and the other behind (called Trojan camp). In the first stage of the mission, after two near-Earth flybys, Lucy will head onto the Greek camp to visit between 2027 and 2028 four of its asteroids: Eurybates, Polymele, Leucus and Orus. In the second stage of the mission, Lucy will pass by the Earth again to go to the Trojan camp, where it will visit the asteroid Patroclus-Menoetius in 2033. Then, Lucy is expected to cycle between the two Trojan clouds every six years. Figure 1.1 represents the scheduled path Lucy will follow. [4]

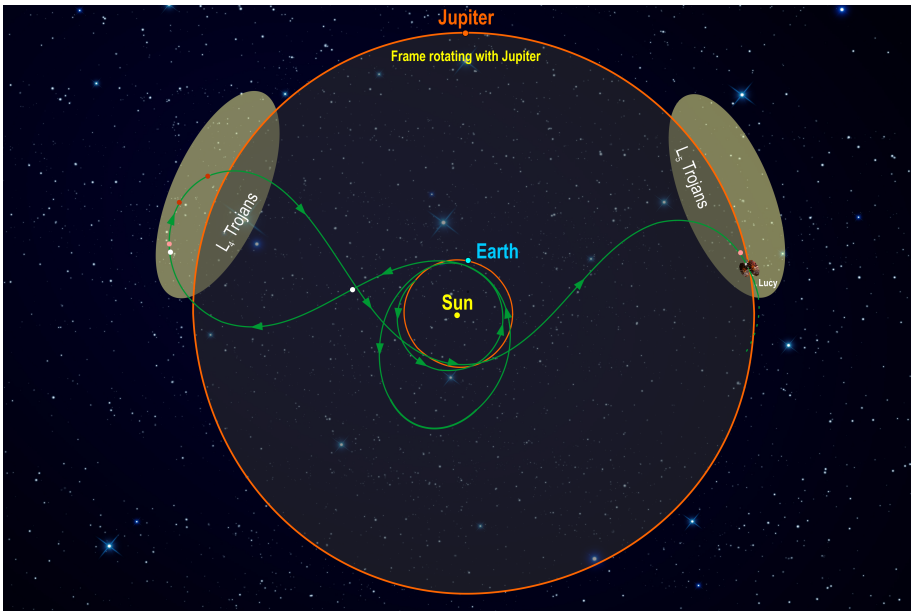

Figure 1.1: Lucy's orbital path. The spacecraft's path is depicted in green, Greek camp is on the left and Trojan camp to the right.[5]

1.3 Economic Context

From observing space with the naked eye to the space telescope Hubble, humans have progressed greatly. But the fastest progress took place during the Cold War, when space projects enjoyed almost unlimited funding. For example, between 1958 and 1966, NASA budget raised from 0.1% up to 4.4% of the US Federal Budget. Overall, it increased from 732 millions to 43,554 millions, which is an increase of 42,822 millions in just 8 years.

After the Apollo program the budget has been decaying over the years until reaching a steady 0.5% for these last years, which is similar to the budget of 1960. For 2018, NASA has a budget of 19,092 millions [6]. In any engineering project, costs and efficiency are important, but this is vital when talking about space projects due to the costs inherent to them.

Space mission costs are typically divided in three phases: design and construction of the spacecraft, the launcher and launch costs and the operation cost during the mission life. One of the most expensive phase is the launch phase, potentially gathering 30-40% of the total mission cost. So, improvements in this stage decrease effectively the total cost of the space mission. This is huge for the future of the space industry because it means that it cannot be only developed by governments agencies (such as NASA

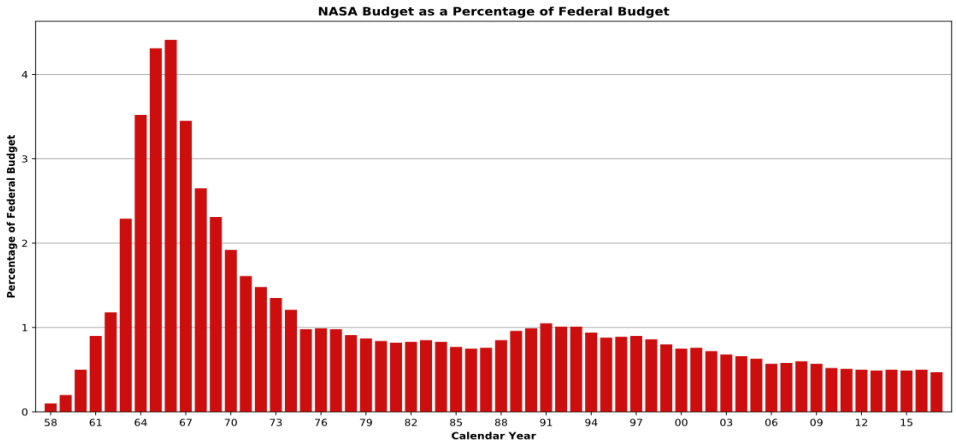

Figure 1.2: NASA's budget as percentage of federal total, from 1958 to 2017. [7]

or ESA), but for the first time it becomes an industry accessible for private companies. More companies in the space industry means more competitiveness, which immediately translates in a faster technology development. Figure 1.3 shows the rapid growth of space industry over the last years.

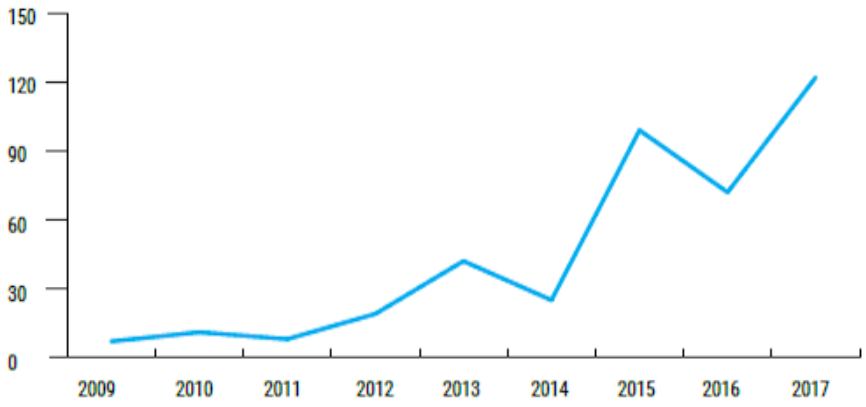

Figure 1.3: Venture capital invested in the space industry since 2009.[8]

Nowadays, on 2018, there are more than 800 private space companies. Approximately ten are the main companies working on asteroid mining, and a handful others are developing technology for this purpose (for example, ispace, founded on 2013, specializes in robotics rovers cheap to put in space). The top three asteroid mining private companies nowadays could very well be Deep Space Industries, Planetary Resources and TransAstra. Their ef-

forts at the moment are focused on developing the technology necessary to explore and analyze asteroids, in order to separate the ones with the best mission profit ratio (it is estimated that profit of near-Earth objects and asteroids could fluctuate from one to thirty five billion US$). This year, on January 2018, Planetary Resources put in orbit its Arkyd-6 Satellite, intended to find water on near-Earth asteroids. [9]

It is important to note the repercussion the space industry is having on the global market, even though it can be considered to have begun just only 15 years ago, which gives a first insight of the potential this industry has.

1.4 Orbital maneuvers

A space mission is limited by the amount of propellant the spacecraft has because once it runs out of fuel, the mission ends. For this reason it is important to minimize the fuel expenditure during cruise phases, this way the spacecraft has more propellant for its nominal operations.

There are a few things that can be done about this, for example finding an adequate launch window with a good configuration of the planets or asteroids of interest for the mission. It is possible to save up to 50% of fuel with the proper launch day. But there is another important decision to make in the design of a mission, the orbit maneuvers.

In order to perform an orbit maneuver, a delta-v, Δv is required. In space flight dynamics, Δv is a measure of the impulse needed to complete an orbital maneuver. This Δv can very well imply a velocity change in the velocity magnitude (pumping maneuver), direction (cranking maneuver), or both. By definition,

$$\Delta v = \int_{t_0}^{t_1} \frac{|T(t)|}{m(t)} dt$$

where where T(t) is the instantaneous thrust at time, t and m(t) is the instantaneous mass at time, t. Because a spacecraft follows the basic principles of a rocket (it is a device that accelerates by expelling part of its mass) then the Tsiolkovsky rocket equation relates Δv with the mass of the spacecraft as follows:

$$\Delta v = v_e * \ln\left(\frac{m_0}{m_f}\right)$$

where m_0 is the initial mass, m_f is the final mass and v_e is the velocity of the exhaust gas, $v_e = g_0 I_{sp}$ with I_{sp} as specific impulse and g_0 as the standard gravity.

The magnitude of Δv is related to the variation of the spacecraft mass (this variation is obviously negative, due to the propellant being consumed) by:

$$\frac{\Delta m}{m_0} = 1 - e^{-\frac{\Delta v}{I_{sp} g_0}} \tag{1.1}$$

This equation can be applied only to impulsive orbital maneuvers where engines are able to apply the Δv instantaneously. If the thrust cannot be considered instantaneous, for example in low-thrust maneuvers, the equation loses precision due to gravity effects not being taken into account during the maneuver duration. In these cases, a more complicated analysis is required, based on the integration of thrust and the spacecraft's state vector. The concepts of impulsive transfers and low-thrust transfers will be introduced next, and studied more in depth in chapter 2.

Firstly, impulsive maneuvers. These maneuvers involve an instantaneous Δv produced by the on-board rocket motors. During the maneuver, the position of the spacecraft is considered constant due to the brief period of time the maneuver lasts.

Secondly, gravitational assisted maneuvers. This maneuver was firstly used in 1959 to photograph the far side of the Earth's Moon. It takes advantage of the relative movement and gravity of a celestial body to change the speed of the spacecraft, saving propellant. When the spacecraft flies near a planet there is an energy exchange between them. However, because of the difference in their masses, the change in the planet's orbit is negligible but the spacecraft experiments a change in its velocity. These maneuvers are used as much as possible to reduce propellant consumption, so most of the mission involve flybys.

Lastly, the low-thrust maneuvers. They are also called non-impulsive maneuvers, but this name is often misleading. This type of maneuver involves a relatively low impulse but applied over a long period of time. They are specially useful when power is limited and they are often faster and less propellant-consuming than conventional propulsion maneuvers.

The possibility of performing one orbital maneuver or the other depends on the resources available and in the propulsion system the spacecraft has. Impulsive maneuvers are carried out by chemical engines due to their characteristics, a high thrust applied almost instantaneously. Low-thrust maneuvers and flybys (gravitational assisted maneuvers) are performed by electrical engines, because their low but continuous thrust. The propulsive systems will be discussed in the following section.

1.5 Propulsive systems

A very important parameter of any engine or propulsive system is the specific impulse, I_{sp}. The specific impulse is the total impulse per unit of propellant consumed, or in other words, it is a measure of how effectively a rocket uses the propellant. In general, the specific impulse is calculated as:

$$I_{sp} = \frac{F_{\text{thrust}}}{g_0 \dot{m}} = \frac{v_e}{g_0} \tag{1.2}$$

where F_{thrust} is the thrust generated by the engine, g_0 is the sea-level standard acceleration of gravity, $\dot{m}$ is the mass flow rate and v_e is the average exhaust speed along the axis of the engine. The second expression is most commonly used in rocketry. I_{sp} is measured in seconds.

Depending on the type of propellant and the way of generating thrust, rocket engines can be classified in chemical engines and low-thrust engines.

Chemical engines

Chemical engines are the most used propulsive system. Thrust is usually generated by combustion, although there are a few non-combusting engines. The last ones work by releasing compressed gas through the nozzle. Combustion engines work by the action-reaction Newton principle. There is a propellant (solid, liquid or gas) that when combustion happens reaches a high pressure, high temperature state. When this exhaust goes through the nozzle it is accelerated to supersonic speeds and so, the rocket experiments this acceleration but in the opposite direction of the exhaust exit. Rocket engines are the most powerful and lightest engines, but in exchange they are the least propellant-efficient as well.

An alternative to chemical engines are thermal and nuclear engines. Its principle is similar to chemical engines, but the high temperature of the propellant is obtained by a power source, such as electric or nuclear power instead of a chemical reaction (combustion). Their specific impulse is around 825-925 seconds.

Table 1.1 shows different types of chemical engines in terms of propellant and their correspondent specific impulse, I_{sp}. Solid rocket boosters deliver high-thrust with low specific impulses, so they are ideal for launch vehicles. They are cheaper than liquid propellant rockets but once ignited the combustion process cannot be stopped. Liquid propellant rockets can be turned on and off, so they are the ones used for impulsive space maneuvers.

Propellant	$\mathbf{I_{sp}}[s]$
Cold gas (carbon dioxide)	50
Monopropellant hydrazine	230
Solid rocket (STS booster)	250
Nitric acid/monomethylhydrazine	310
Liquid oxygen/liquid hydrogen	455

Table 1.1: Chemical engines and their specific impulse.[10]

Recalling equation 1.1 for chemical engines, it is easy to see that, when high impulses are required (a large Δv) and the specific impulse is low (chemical engine characteristic), a big amount of propellant needs to be burnt. For example, changes in velocity on the order of 1 km/s would require over 25% of the spacecraft mass on propellant.[10]. Due to limitations on the payload, just a certain quantity of chemical fuel can be carried on the spacecraft, limiting greatly the usage of these engines, which sometimes constitutes a big disadvantage for chemical engines. The main advantage is the instantaneous high thrust they offer.

Low-thrust engines

In the group of low-thrust propulsive systems, there are different ways of producing the thrust. Some of them are:

Ionic propulsion: it generates thrust by accelerating positive ions (atoms or molecules charged electrically). The acceleration of ions comes from the Coulomb force along an electric field. Following the momentum conservation, when these ions are accelerated, the spacecraft suffers an acceleration of equal magnitude but opposite direction. The most common propellant is xenon because it is easily ionized, has a high atomic mass, is inert and has a high storage density.[11]

Solar sail: it uses radiation pressure to generate thrust. Photons are the particles the light is made of, and each photon has a momentum given by $p = E/c$. Thrust can be generated by changing this momentum direction. This can be achieved by using mirrors (solar sails) made of metallised plastic film. An 800x800m solar sail can generate up to 5N at Earth distance from the Sun, which is great enough if used continuously. The big advantage of this propulsion system is that no propellant has to be carried or stored in the spacecraft. It has yet to solve some technical difficulties to consider it a viable option.[12]

Electromagnetic propulsion: it generates thrust by accelerating plasma charged particles and expelling them, a similar principle as ionic propulsion. A conductive propellant (usually xenon) is injected into a chamber with an electromagnetic field inside. Electrons trapped in the field ionize the propellant particles, which then are accelerated by action of the electromagnetic field.[13]

In table 1.2 the specific impulse of electric and electromagnetic propulsion system is shown. For the solar sail propulsion system it is easy to deduce that, because no propellant is consumed, $\dot{m} = 0$, and so, from equation 1.2 follows $I_{sp} = \infty$. All these propulsion systems have in common their high specific impulse. This means that they are able to generate thrust with tiny amounts of propellant, but this thrust, because is related to the mass flow through the engine, is very low. In other words, using tiny amounts of propellant also means having low thrust.

Engine type	**Specific impulse**, I_{sp}	**Thrust**, N
Electrothermal (ARCJET)	800-1200	$10^{-2} - 10$
Electromagnetic (MPD)	2000-5000	100
Electrostatic (ION)	3500-10000	0.5

Table 1.2: Specific impulse for different types of rocket engines [14].

To sum all up, the specific impulse is closely related to the orbital maneuver that can be performed. Chemical engines can generate a tremendous amount of thrust almost instantly (around $10^7 N$), but in exchange they consume a lot of propellant (recall from table 1.2 that they had the lowest specific impulse). Because of this characteristic, this propulsion system is associated with impulsive maneuvers.

On the other hand, low-thrust propulsion (ION, ARCJET and MPD) is less propellant consuming, but the amount of thrust it can generate is insignificant when compared with chemical propulsion. This is why they are best suited for low-thrust maneuvers, where the engines are powering the aircraft for longer periods of time in order to reach the desired Δv. In exchange, the amount of propellant consumed is very low (recall the high specific impulse from this type of propulsion system).

1.6 Outline of the document

This thesis has been organized as follows:

Chapter 1 has introduced the possible applications of the results of this thesis, asteroid mining and asteroid research. It has given an historical and economical insight of the actual state of space missions to asteroids, to then introduce the basic concepts needed in order to understand the design choice of the thesis, low-thrust trajectories.

Chapter 2 has treated with the two-body problem, a classical and simplified problem about the dynamics and behaviour of bodies in space. Then, the basic concepts of impulsive transfers and low-thrust transfers, which were also introduced at the end of the previous chapter, are explained more in depth to justify the choice of low-thrust over high impulsive thrust.

Chapter 3 develops all the theory behind the generalized logarithmic spirals method. It sets out the initial problem and explains how to solve it. Then, it analyzes the results, distinguishing three families of solutions based on some characteristics common for each other. These families are the elliptic spirals, the parabolic spirals and the hyperbolic spirals, for which all their correspondent trajectory and time of flight equations are deduced.

Chapter 4 is intended to prove that the results of the analytic solution obtained in the previous chapter are consistent and valid. It is also useful and necessary to make sure that the code that will be used in this thesis works perfectly, so the results obtained from it are consistent with the theory.

Chapter 5 lays out the Lambert's problem of finding the orbit that connects Earth with the asteroid belt. It does so using the generalized logarithmic spirals that this whole thesis is based on.

Lastly, chapter 6 gives an overall vision of the thesis and suggests future work lines to further develop and improve this thesis.

Chapter 2

Dynamical Model

"I used to measure the skies,
now I measure the shadows of Earth.
Although my mind was sky-bound,
the shadow of my body lies here."
-Johannes Kepler
Epitaph he composed for himself a few months before he died

Classical mechanics defines the two-body problem as the motion of two massive point particles that interact only with each other in absence of any force, but the gravitational force inherent to the mass.

In the first section of this chapter, a vector-based approach to this classical problem is presented in order to determine the motion between the two bodies.

Although short and simple, this section will settle the principles of our equations of motion. Also, it will obtain the dynamic equation that will be used in chapter 4 to validate the analytic solution of the *generalized logarithmic spirals*.

As for the second section of the chapter, impulsive transfers will be analyzed more precisely and the Hohmann Transfer will be introduced.

Finally, in the third section of this chapter, low-thrust transfers are briefly explained, introducing the method chosen to solve the Lambert problem in this thesis and setting the discussion about the reasons for using this method.

2.1 The Two-Body Problem

Equations of Motion in an Inertial Frame

From now on, any given vector $\vec{a}$ will be declared in a bold font $\mathbf{a}$, therefore,

$$\vec{a} \equiv \mathbf{a}, \quad \left|\vec{a}\right| \equiv a$$

Imagine two point masses, m_1 and m_2, acted upon the force of gravity as figure 2.1 depicts. Their mass center is fixed to a inertial frame of reference. Because of the gravitational attraction of each other, m_2 exerts a force $\mathbf{F}_{12}$ to m_1, and vice versa with force $\mathbf{F}_{21}$.

Also, denote $\hat{\mathbf{u}}_r = \frac{\mathbf{r}}{r}$ as the unit vector that goes from m_1 to m_2, and $\mathbf{r} = \mathbf{R}_2 - \mathbf{R}_1$ as the position vector of m_2 relative to m_1. They are depicted in figure 2.1 as well.

The position vector $\mathbf{R}_G$ can be defined as

$$\mathbf{R}_G = \frac{m_1\mathbf{R}_1 + m_2\mathbf{R}_2}{m_1 + m_2}$$

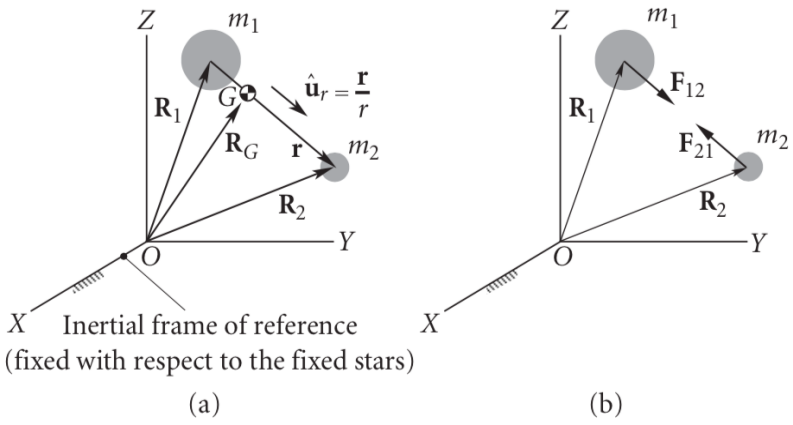

Figure 2.1: (a)Two masses in an inertial frame. (b)Free-body diagrams.[15]

and so, the absolute (because it measured respect to the intertial frame) velocity and acceleration:

$$\mathbf{v}_G = \dot{\mathbf{R}}_G = \frac{m_1\dot{\mathbf{R}}_1 + m_2\dot{\mathbf{R}}_2}{m_1 + m_2}$$
$$\mathbf{a}_G = \ddot{\mathbf{R}}_G = \frac{m_1\ddot{\mathbf{R}}_1 + m_2\ddot{\mathbf{R}}_2}{m_1 + m_2}$$

Gravitational force is one of the most well-known equations in Physics. Its expression is as follows:

$$\mathbf{F} = G\frac{m_1 m_2}{r^2}\hat{\mathbf{u}}_r \tag{2.1}$$

If no other forces act upon these masses, they will attract each other accordingly with the following forces:

$$\mathbf{F}_{12} = G\frac{m_1 m_2}{r^2}\hat{\mathbf{u}}_r \tag{2.2}$$
$$\mathbf{F}_{21} = G\frac{m_1 m_2}{r^2}(-\hat{\mathbf{u}}_r) \tag{2.3}$$

being $\mathbf{F}_{12}$ the force exerted on m_1 by m_2, and $\mathbf{F}_{21}$ the same force magnitude but exerted on m_2 by m_1, as stated at the beginning of the chapter.

If we now recall Newton's Second Law of Motion, the force on the body of mass m_2 follows:

$$\mathbf{F}_{21} = m_2\ddot{\mathbf{r}}_2 \tag{2.4}$$

and combining equations 2.3 and 2.4 it is obtained:

$$G\frac{m_1 m_2}{r^2}(-\hat{\mathbf{u}}_r) = m_2\ddot{\mathbf{r}}_2 \tag{2.5}$$

and equivalently for the mass m_1:

$$G\frac{m_1 m_2}{r^2}\hat{\mathbf{u}}_r = m_1\ddot{\mathbf{r}}_1 \tag{2.6}$$

The equations 2.5 and 2.6 are the equations of motion of two bodies in inertial space

Equations of Relative Motion

Manipulating equations 2.2 and 2.3 is easy to get:

$$m_1 m_2(\ddot{\mathbf{r}}_2 - \ddot{\mathbf{r}}_1) = -G\frac{m_1 m_2}{r^2}(m_1 + m_2)\hat{\mathbf{u}}_r \tag{2.7}$$

Cancelling $m_1 m_2$ in both sides and noticing that $\ddot{\mathbf{r}}_2 - \ddot{\mathbf{r}}_1 = \ddot{\mathbf{r}}$ it follows:

$$\ddot{\mathbf{r}} = -G\frac{(m_1 + m_2)}{r^2}\overset{\wedge}{\mathbf{u}}_r \tag{2.8}$$

Finally, defining the gravitational parameter $\mu = G(m_1 + m_2)$ and recalling that $\overset{\wedge}{\mathbf{u}}_r = \frac{\mathbf{r}}{r}$, equation 2.8 can be written as:

$$\ddot{\mathbf{r}} = -\frac{\mu}{r^3}\mathbf{r} \tag{2.9}$$

2.2 Impulsive Transfers

As it was introduced in section 1.4, an impulsive transfer or impulsive maneuver is the use of a propulsion system to change the direction or the orbit of a spacecraft. The main characteristic of an impulsive transfer is the amount of time the engine is providing thrust. This time, ideally, should be instantaneous, so the position of the spacecraft during the time the impulse is being exerted can be considered constant. This way, the maneuver can be considered as a two-body problem (explained in the previous section 2.1), avoiding this way the term of the rocket thrust when solving the equations of motion (equation 2.3). Because engines need to provide thrust for a few minutes, the assumption above is applied if this time can be considered negligible when compared to the duration of the total mission, usually the case for high-thrust rockets with short burn times. Engines capable to provide such impulse are chemical engines.

Impulsive transfers are suited for missions or maneuvers where little transfer time is required (for example manned missions or for lifting off from the Earth, which require a rapid change in velocity). But because their propellant limitation, there are a certain number of impulsive transfers a spacecraft can perform, so they need to be planned carefully.

Hohmann Transfer

When talking about impulsive transfers, mentioning the Hohmann transfer is a must. Hohmann transfer is the most energy efficient two-impulse maneuver when transferring between two coplanar circular orbits. It follows an elliptic orbit tangent to the circular orbits at its apse line (ilustrated in figure 2.2). Obviously, to transfer from one orbit to the other, only one half of the ellipse has to be followed.

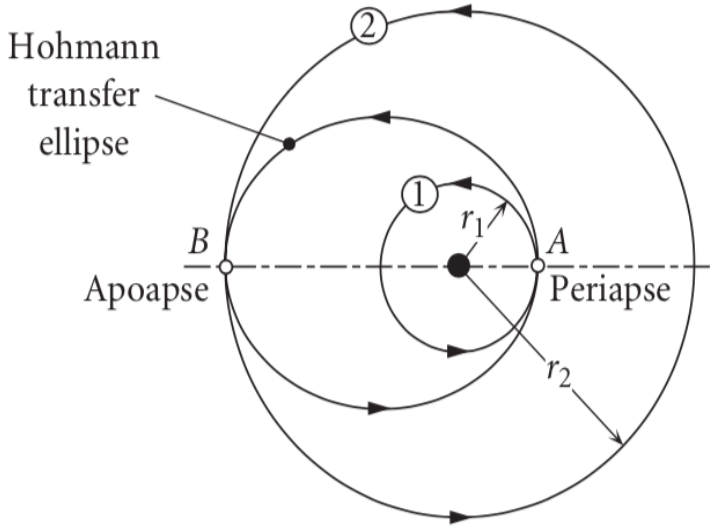

Figure 2.2: Hohmann transfer diagram.[10]

The energy of an orbit depends only on its semimajor axis, a. For an ellipse, the specific energy is negative (this result will be obtained in chapter 3) and follows:

$$\mathcal{E} = -\frac{\mu}{2a}$$

Therefore, to increase the energy, one must make $\mathcal{E}$ less negative by increasing a. This means that orbits with larger semimajor axis will have more energy, and so, in figure 2.2 energy increases as approaching the outer circle. If a spacecraft is located at point A, in order to move to the outer circular orbit 2, a Δv_1 is required. If nothing else is done, the spacecraft will continue flying over the Hohmann transfer so a Δv_2 is needed to finally place the spacecraft in orbit 2. The total impulse is $\Delta v_{TOTAL} = \Delta v_1 + \Delta v_2$. If the spacecraft were in point B the same problem would apply. Although this time the energy would decrease during the trajectory, the same amount of Δv_{TOTAL} would be required, but instead of accelerating the spacecraft, this impulse would be spent on decelerating it.

2.3 Low-Thrust Transfers

Low-Thrust Transfers are also called Non-Impulsive Transfers. This kind of transfer, unlike impulsive transfers, involve continuous thrust. Because of

the long duration this thrust is applied over, the thrust acceleration during the transfer maneuver cannot be longer negligible. This means that the spacecraft changes its velocity gradually, so the trajectory usually degenerates in a spiral trajectory. Also, because of the long time the engines are on, the engine's thrust (which will be referred as a perturbing acceleration)has now to be taken into account. Therefore, the dynamic of a spacecraft with a low-thrust propulsive system will follow equation 2.9 with the thrust acceleration added to it. This perturbing acceleration, in its most general form, follows:

$$\mathbf{a}_p = \frac{\mu}{r^2}\left[\xi \cos\psi \mathbf{t} + (1-2\xi)\sin\psi \mathbf{n}\right]$$

with ξ as the control parameter, μ as the standard gravitational parameter and ψ as the flight-direction angle. Low-thrust transfers are the best, and sometimes the only option to interplanetary missions such as Deep Space or the previous mentioned Dawn. It has also a lot of potential for placing geostationary satellites in orbit due to the high altitude of its orbit, which is pretty difficult to reach with a more direct method. Also, because low-thrust transfers use much less propellant, the spacecrafts and satellites have more propellant left after reaching their final destination, increasing its operational life. The downside of this method is that, because the engines are turned on for almost all the transfer process, the engine's steering and throttling need to be determined completely, which constitutes a complex optimization problem.

This optimization problem can be solved by different methods. However, all of them need an initial guess which sometimes is difficult to obtain, and having a good initial guess does not even guarantee the convergence to an optimal solution, particularly when the optimization problem is applied to multiple low-thrust operations. Shape-based methods are a different approach to the problem with some advantages to the optimal problem just mentioned, which gives the method a great potential for exploring large spaces of solutions in the mission design stage. The shape-based method chosen for this thesis is the generalized logarithmic spirals for the preliminary design of low-thrust trajectories. All of this will be explained in chapter 5.

Chapter 3

Generalized Logarithmic Spirals

"Although changed, I shall arise the same"
-Jakob Bernoulli

SHAPE-BASED method has proven to be extremely useful for low-thrust preliminary trajectory design, and so it is becoming the most preferable approach for low-thrust analysis. Instead of directly integrating the equations of motion given a thrust profile, the shape of the trajectory is assumed a priori, and then the thrust profile required to follow the shape is obtained.

This shape-based approach was conceived for providing suitable initial guesses for more sophisticated algorithms for trajectory optimization, which are usually complicated to obtain otherwise.

In this chapter, as Javier Roa [16] firstly did, the equations of motion are going to be solved without any assumption about the shape of the trajectory. Solving them rigorously will lead to an entire family of curves that is called *Generalized Logarithmic Spirals, S*.

The integrals of motion that will be studied in this chapter will lead to a natural classification of the trajectories: elliptic, parabolic and hyperbolic spirals. These spirals will be analyzed thoroughly in a following section, but only the elliptic and parabolic spirals will be used.

3.1 The equations of Motion.

Rather than considering that the particle is only influenced by a central gravitational acceleration, it is more interesting adding a perturbing acceleration (for example, the ΔV of a spacecraft) that affects the particle as well.

Therefore, using the equation 2.9 the new dynamic of the particle follows:

$$\ddot{\mathbf{r}} + \frac{\mu}{r^3}\mathbf{r} = \mathbf{a}_p \tag{3.1}$$

being the perturbed acceleration $\mathbf{a}_p$, as Bacon proved [17]:

$$\mathbf{a}_p = \frac{\mu}{2r^2}\cos\psi\mathbf{t} \tag{3.2}$$

where ψ is the flight direction angle and $\mathbf{t}$ is the vector tangent to the trajectory, so it can be expressed as $\mathbf{t} = \frac{\mathbf{v}}{v}$

Equation 3.1 will be useful in the validation chapter of this thesis. In what follows the problem is normalized so that $\mu = 1$.

Some approaches would consider ψ constant, but in order to keep the rigour in the solution, ψ will not be considered constant.

In this thesis, the perturbing term will be confined to the orbital plane, so the problem becomes planar and can be described by polar coordinates (r, θ).

It is of interest to consider an orbital frame $\mathcal{L} = \{\mathbf{i},\mathbf{j},\mathbf{k}\}$ given by the usual definition:

$$\mathbf{i} = \frac{\mathbf{r}}{r}, \quad \mathbf{k} = \frac{\mathbf{h}}{h}, \quad \mathbf{j} = \mathbf{k} \times \mathbf{i} \tag{3.3}$$

where the angular momentum vector is $\mathbf{h} = \mathbf{r} \times \mathbf{v}$. The velocity of the particle in the orbital frame $\mathcal{L}$ would be:

$$\mathbf{v} = \dot{r}\mathbf{i} + r\dot{\theta}\mathbf{j} \tag{3.4}$$

Also, the problem can be formulated using the intrinsic frame $\mathcal{T} = \{\mathbf{t},\mathbf{n},\mathbf{b}\}$ in terms of the tangent, normal and binormal vectors respectively. They can be expressed in the orbital frame as:

$$\mathbf{t} = \frac{1}{v}(\dot{r}\mathbf{i} + r\dot{\theta}\mathbf{j}), \quad \mathbf{n} = \frac{1}{v}(\dot{r}\mathbf{i} - r\dot{\theta}\mathbf{j}), \quad \mathbf{b} \equiv \mathbf{k} \tag{3.5}$$

The tangent vector can be alternatively defined in terms of the flight-direction angle ψ:

$$\mathbf{t} = \cos\psi\mathbf{i} + \sin\psi\mathbf{j} \tag{3.6}$$

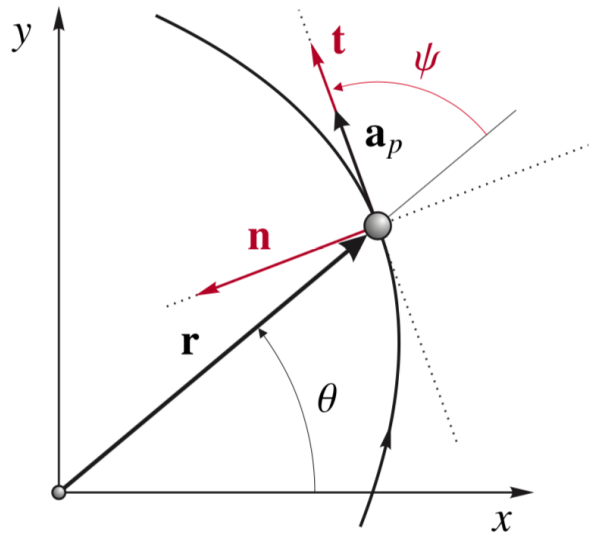

Figure 3.1: Geometry of the problem.[16]

Comparing equations 3.5 and 3.6 it follows:

$$\cos\psi = \frac{\dot{r}}{v}, \quad \sin\psi = \frac{r\dot{\theta}}{v}, \quad \tan\psi = r\frac{d\theta}{dr} \tag{3.7}$$

The forces acting on the particle, as it was stated at the beginning of this section, are the gravitational attraction of the central body, $\mathbf{a}_g$, and the perturbing acceleration $\mathbf{a}_p$ of equation 3.2. If they are expressed in $\mathcal{T}$:

$$\mathbf{a}_g = -\frac{1}{r^2}(\cos\psi\mathbf{t} - \sin\psi\mathbf{n}), \quad \mathbf{a}_p = \frac{\cos\psi}{2r^2}\mathbf{t} \tag{3.8}$$

The intrinsic equations of motion turn out to be:

$$\frac{dv}{dt} = -\frac{\cos\psi}{2r^2}, \quad v^2\kappa = \frac{\sin\psi}{r^2} \tag{3.9}$$

where κ is the curvature of the trajectory. It relates to the arclength s by means of:

$$\kappa = \frac{d}{ds}(\psi + \theta) \quad \text{and} \quad v = \frac{ds}{dt} \tag{3.10}$$

Combining these identities in the last equation 3.10 with equations 3.9 and remembering the geometric relations in equations 3.7 yields the final form of the equations of motion. The equations reduce to:

$$\frac{dv}{dt} = -\frac{\cos\psi}{2r^2} \tag{3.11}$$

$$\frac{d}{dt}(\psi + \theta) = \frac{\sin\psi}{r^2} \tag{3.12}$$

$$\cos\psi = \frac{\dot{r}}{v} \tag{3.13}$$

$$\sin\psi = \frac{r\dot{\theta}}{v} \tag{3.14}$$

and they must be integrated from the initial conditions

$$t = 0: \quad v = v_0,\ \psi = \psi_0,\ r = r_0,\ \theta = \theta_0$$

The equation of energy

Let $\mathcal{E}_k$ denote the specific Keplerian energy of the system, defined as

$$\mathcal{E}_k = \frac{v^2}{2} - \frac{1}{r}$$

Its time evolution is given by the power performed by the perturbing acceleration

$$\frac{d\mathcal{E}_k}{dt} = \mathbf{a}_p \cdot \mathbf{v}$$

From equation 3.2 it follows:

$$\frac{d\mathcal{E}_k}{dt} = \frac{\cos\psi}{2r^2}(\mathbf{t} \cdot \mathbf{v}) = \frac{v\cos\psi}{2r^2}$$

The geometric relation between the radial velocity and $\cos\psi$ (equation 3.13) yields an equation with separate variables,

$$\frac{d\mathcal{E}_k}{dt} = \frac{1}{2r^2}\frac{dr}{dt} \longrightarrow \frac{d\mathcal{E}_k}{dr} = \frac{1}{2r^2}$$

which is integrated to provide the first integral of motion:

$$d\mathcal{E}_k = -\frac{1}{2r} + \frac{K_1}{2} \longrightarrow v^2 - \frac{1}{r} = K_1 \tag{3.15}$$

Here K_1 is a constant of integration, which depends on the initial values of the radius and velocity r_0 and v_0 by:

$$K_1 = v_0^2 - \frac{1}{r_0} = v^2 - \frac{1}{r} \tag{3.16}$$

The sign of K_1 (negative,zero or positive) will fully determine the type of spiral (elliptic, parabolic or hyperbolic respectively). Therefore, the initial radius and velocity determines the type of trajectory an object will follow. Another conclusion can be drawn from this equation. As the velocity is squared, for the velocity to be real a lower bound for K_1 can be found:

$$K_1 \geq -\frac{1}{r} \longrightarrow 1 + K_1 r \geq 0 \tag{3.17}$$

The equation of the angular momentum

There is another first integral, this time related to the angular momentum. Dividing equation 3.11 by 3.12 and introducing equation 3.7c it can be obtain:

$$\frac{dv}{v} = -\frac{cot\psi}{2}(d\psi + d\theta) = -\frac{dr}{2r} - \frac{1}{2}cot\psi d\psi$$

which is integrated easily,

$$2\ln v = -\ln r - \ln(\sin\psi) + \ln K_2 \longrightarrow v^2 r \sin\psi = K_2 \tag{3.18}$$

considering $\sin\psi > 0$. This result defines a new integral of motion, that in terms of the constant K_2 can determined from the initial values r_0, v_0, ψ_0:

$$K_2 = v_0^2 r_0 \sin\psi_0 = v_0 r_0^2 \dot{\theta}_0 \tag{3.19}$$

Similar to K_1, it can also be calculated with non-initial values:
$K_2 = v^2 r \sin\psi$

The integral of motion is the generalization of the angular momentum equation. It relates to the angular momentum of the Keplerian orbit at r, h_k, by means of:

$$\frac{v_k \sin\psi_k}{v^2 \sin\psi} = \frac{h_k}{K_2}$$

An interesting property of the generalized spiral can be drawn from the form of equation 3.19: since $\sin\psi_0$ is symmetric with respect to $\psi_0 = \pi/2$, two different trajectories that emanate from the same radius and with the same value of K_1 and K_2 can be found. The first trajectory will depart in

lowering regime and the second in raising regime while sharing the same value of $K2$. These two trajectories relate to the two different *regimes* that characterize the generalized spirals considered in this chapter. The radius of the orbit will increase/decrease depending on the sign of $\dot{\mathbf{r}}$. Since $\psi \in (0, \pi)$, equation 3.13 shows that there are two possibilities:

- *RAISING REGIME*: corresponding to $\cos\psi > 0$ ($\dot{r} > 0$)
- *LOWERING REGIME*: corresponding to $\cos\psi < 0$ ($\dot{r} < 0$)

In raising regime the perturbing acceleration $\mathbf{a}_p$ moves the particle away from the attracting body (the origin). However, in lowering regime the opposite happens.

The flight-direction angle ψ

From equation 3.19 and taking into account the energy equation 3.16 the value of $\sin\psi$ takes the form:

$$\sin\psi = \frac{K_2}{rv^2} = \frac{K_2}{1 + K_1 r} \tag{3.20}$$

This relation is the solution to the differential equation

$$\frac{d\psi}{dr} = -\frac{K_1}{rv^2}\tan\psi \quad \text{or} \quad \frac{d\psi}{dr} = -\frac{K_1}{rv}\sin\psi \tag{3.21}$$

that governs the evolution of the flight angle ψ. Note that for $K_1 = 0$ the angle ψ would be constant, so the trajectory would reduce to a logarithmic spiral. An important conclusion to take from here is that if $K_1 < 0$ the flight-direction angle will always grow in time, and for $K_1 > 0$ it will decrease.

Also, from equation 3.20 $\cos\psi$ can be defines as:

$$\cos\psi = \pm\frac{\sqrt{(1 + K_1 r)^2 - K_2^2}}{1 + K_1 r} \tag{3.22}$$

The $\pm$ sign relates to the raising/lowering regime of the trajectory. Considering equations 3.20 and 3.22 an expression for $\tan\psi$ can be written:

$$\tan\psi = \pm\frac{K_2}{\sqrt{(1 + K_1 r)^2 - K_2^2}} \tag{3.23}$$

3.2 Families of solutions

Similar to $\mathcal{E}_k$ in the Keplerian case, different values of the constant (K_1 in the generalized logarithmic spirals), yield different types of solutions. The resulting families will be briefly introduced as it was promised before.

ELLIPTIC SPIRALS ($K_1 < 0$)*:* Their main characteristic is that they have a maximum radius so they never escape to infinity. Because the generalized energy is negative, the flight-direction angle always grows, as it was mentioned before.

Another property to take into account is that, if the orbit is initially in lowering regime (this is $\psi_0 > \pi/2$ and $\cos\psi_0 < 0$), the orbit will fall until reaching the origin (which is the body the object is orbiting around). Therefore, an orbit that is initially in lowering regime is $r = 0$.

On the other hand, if the orbit is initially in raising regime (this is $\psi_0 < \pi/2$ and $\cos\psi_0 > 0$), it will reach its maximum radius when the flight-direction angle $\psi = \pi/2$, to then enter lowering regime. This is easy to see taking into account that, despite $\cos\psi$ being positive when in raising regime, from the moment $\psi = \pi/2$ is reached, $\cos\psi$ changes its positive sign to negative, changing also the sign of the radial velocity, which translates in $\dot{r} < 0$ sign, which is the lowering regime condition. This maximum radius value will be calculated later in this chapter, as well as others relevant formulas for this type of spiral.

PARABOLIC SPIRALS ($K_1 = 0$)*:* This type of spiral is equivalent to the logarithmic spirals. The velocity coincides with the circular velocity $v = \sqrt{1/r}$ and thus parabolic spirals reach infinity with zero velocity. It is interesting in this spirals to analyze the flight-direction angle. From equation 3.21 and considering $K_1 = 0$ it simplifies to:

$$\frac{d\psi}{dr} = 0 \tag{3.24}$$

which yields an important result. In parabolic spirals the flight-direction angle ψ is constant, and its value will be calculated in the parabolic spiral section of this thesis.

HYPERBOLIC SPIRALS ($K_1 > 0$)*:* When in raising regime, this spirals are able to reach infinity with a nonzero finite velocity $v_\infty = \sqrt{K_1}$. On the contrary to elliptic spirals, spirals of this type have a positive

generalized energy, thus the angle ψ always decreases as it was proved before from equation 3.21. To finish with the hyperbolic spirals, there are two subfamilies depending on the K_2 value:

. *Hyperbolic spirals Type I* $K_2 < 1$: They only have one asymptote.

. *Hyperbolic spirals Type II* $K_2 < 1$: They have two asymptotes.

Both Type I and Type II are separated from the case $K_2 = 1$, that will be explained later on.

For a more graphical distinction of these spirals, see Figure 3.2.

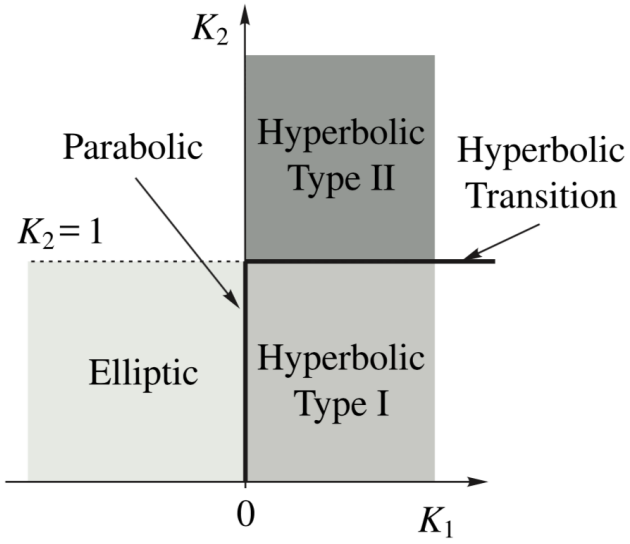

Figure 3.2: Types of spirals in the parametric space (K_1, K_2).[16]

As it can be seen, elliptic spirals exist for $K_1 < 0$ and $K_2 \in (0, 1)$; parabolic spirals exist for $K_1 = 0$ and $K_2 \in (0, 1]$(note that they are represented as a line in the figure); and hyperbolic spirals exist for $K_1 > 0$. Also, the two subfamilies of the hyperbolic spirals are represented, as well as the hyperbolic transition $(K2 = 1)$ that it was mentioned before.

Form of the solution

As it was mentioned in the section 3.1 the perturbing term will be confined to the orbital plane, so the problem becomes planar. Thus, three constants define the shape and orientation of the trajectory in the space, and another one relates the position in the orbit with the time.

To be able to integrate the equations of motion (3.11-3.14) the relation between the polar angle and the radial distance, $\theta(r)$ must be obtained. Inverting this equation yields the trajectory $r(\theta)$. Then, the time evolution will be looked for. Normally it is of interest to find $\theta(t)$ through the inverse of $t(\theta)$, so $r(\theta(t))$ can be obtained using the previous relations. But in some cases the equation $t(\theta)$ cannot be inverted explicitly, so $\theta(t)$ must be solved numerically. So, in this thesis, a different approach is taken by searching $t(r)$, from where $t(r(\theta))$ can be obtained. Similarly to Kepler's equation, the equation for the time of flight cannot be inverted analytically.

3.3 Elliptic Spirals

These spirals are defined by $K_1 < 0$. Regarding the constant K_2, from equation 3.20:

$$K_2 = \sin\psi_0(1 + K_1 r_0) < \sin\psi_0 \leq 1 \longrightarrow K_2 \in (0, 1)$$

confining K_2 to the interval (0,1).

In terms of velocity, elliptic spirals have the following boundary:

$$v^2 < \frac{1}{r}$$

Note that, as $v \to 1/r$, or similarly, $K_1 \to 0$, elliptic spirals converge to parabolic spiral.

In addition, as $v \propto 1/r$, it is logical to think that when the maximum radius is reached, a minimum velocity is reached consequently. Its value can be deduced from equation 3.16:

$$v_m = \sqrt{K_1 + \frac{1}{r_{max}}} = \sqrt{\frac{-K_1 K_2}{1 - K_2}} = \sqrt{\frac{K_2}{r_{max}}} \tag{3.25}$$

Elliptic spirals have a maximum radius that limits their distance to the origin. In order to to calculate this r_{max} one can recall equation 3.20. Knowing that the maximum radius is reached when $\psi = \pi/2$:

$$\sin\pi/2 = 1 = \frac{K_2}{1 + K_1 r} \longrightarrow r_{max} = \frac{1 - K_2}{-K1} \tag{3.26}$$

After the spiral reaches the maximum radius, $\cos\psi$ changes its sign and the spiral enters lowering regime naturally, but the opposite is not true. When in lowering regime, an elliptic spiral will not transition to raising regime, it will fall into the origin.

This is why elliptic spirals cannot escape to infinity. Once they transition into lowering regime they will remain in that regime and fall toward the origin. It is safe to say then that an elliptic spiral can only be in raising regime if it is initially in raising regime.

Figure 3.3 demonstrates this conclusion. Note that r_{max} is reached when $\psi = \pi/2$ and $\cos\psi = 0$. After this point, the radius begins to decrease, ψ keeps increasing as expected, and $\cos\psi$ has changed its sign from positive to negative. Therefore, the spiral has changed from raising to a lowering regime.

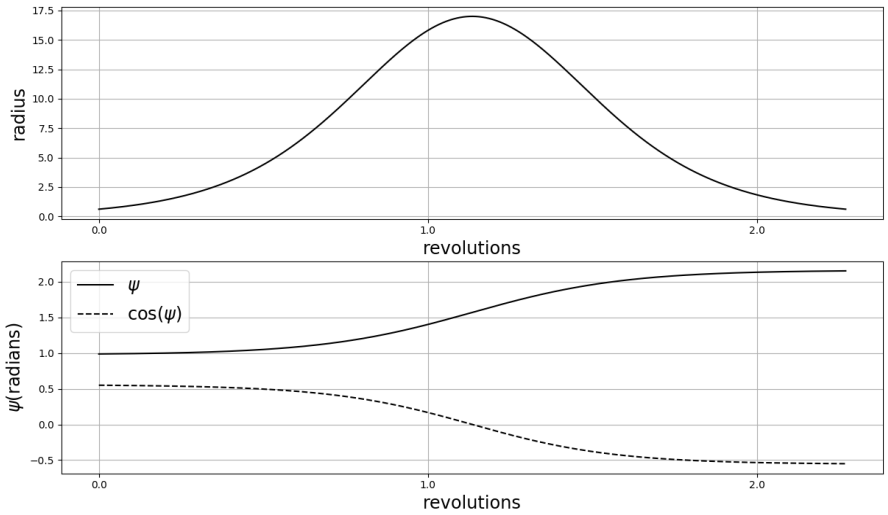

Figure 3.3: Elliptic spiral. Though it is initially in raising regime, it enters lowering regime after reaching r_{max}.

In the remaining of the section the equations of motion are going to be solved for the elliptic case.

The trajectory

When substituting equation 3.23 in equation 3.7c it yields:

$$d\theta = \pm \frac{K_2 dr}{r\sqrt{(1 + K_1 r)^2 - K_2^2}} \tag{3.27}$$

where $\pm$ corresponds to the raising/lowering regime accordingly. If this expression is integrated $\theta(r)$ can be obtained:

$$\begin{aligned}\theta - \theta_m &= \mp\frac{K_2}{l}\left|\arccos\left[\frac{r_{max}}{r}\left(1+\frac{1}{K_2}\right)-\frac{1}{K_2}\right]\right| \\ &= \mp\frac{K_2}{l}\left|\arccos\left[-\frac{1}{K_2}\left(1+\frac{l^2}{K_1 r}\right)\right]\right|\end{aligned} \tag{3.28}$$

with $l = (1 - K_2^2)^{1/2}$. θ_m is a term that defines the orientation of the apoapsis (the point of farthest distance of an orbit), thus $\theta_m = \theta(r_{max})$. Therefore, θ_m is equivalent to the apse-line (the major axis of an ellipse). To calculate θ_m equation 3.28 must be solved for r_0, θ_0:

$$\theta_m = \theta_0 + \frac{K_2}{l}\left|\arccos\left[-\frac{1}{K_2}\left(1+\frac{l^2}{K_1 r_0}\right)\right]\right| \tag{3.29}$$

$$\theta_m^\dagger = \theta_0 - \frac{K_2}{l}\left|\arccos\left[-\frac{1}{K_2}\left(1+\frac{l^2}{K_1 r_0}\right)\right]\right| \tag{3.30}$$

Equation 3.29 applies to spirals initially in raising regime, equation 3.30 corresponds to spirals initially in lowering regime.

In the figures 3.4 and 3.5 two elliptic spirals, one in raising and the other in lowering regime, can be seen. Note that an elliptic spiral in raising regime will always intersect itself at least once (if propagated for sufficient revolutions and with adequate initial conditions). This intersection occur on the axis of symmetry, in $\theta = \theta_m$

The equation for the trajectory, $r(\theta)$ is obtained upon inversion of the equation 3.28:

$$r = r_{max}\frac{1+K_2}{1+K_2\cosh\beta} \tag{3.31}$$

where β denotes the spiral anomaly:

$$\beta = \frac{l}{K_2}(\theta - \theta_m), \quad \beta^\dagger = \frac{l}{K_2}(\theta - \theta_m^\dagger)$$

β corresponds to a spiral initially in raising regime, whereas $\beta^\dagger$ is used for spirals in lowering regime.

The time of flight

In order to fully solve the equations of motion (equations 3.11-3.14) a relation between the position in the orbit and the time is required. The radial velocity, defined in equation 3.13 can be inverted to provide:

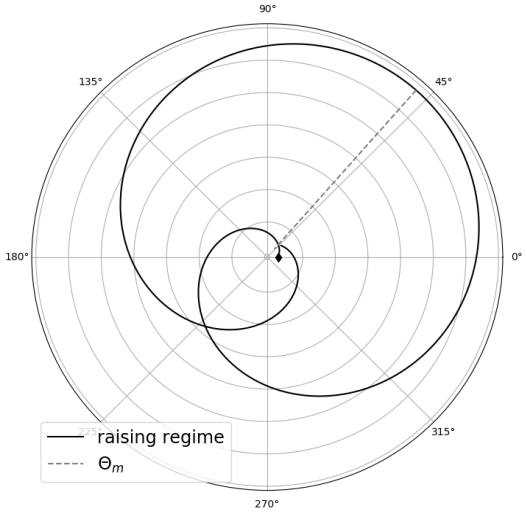

Figure 3.4: A raising elliptic spiral departing from $\diamond$. Note that θ_m also defines the axis of symmetry.

$$\frac{dt}{dr} = \frac{\sec\psi}{v} = \pm\sqrt{\frac{r(1+K_1 r)}{(1+K_1 r)^2 - K_2^2}} \tag{3.32}$$

Now, to obtain the time of flight as a function of the radial distance, $t(r)$, equation 3.32 must be integrated from r_{min} to r:

$$t = t_m \pm \left(\frac{rv}{K_1}\sqrt{\frac{1-\sin\psi}{1+\sin\psi}} + \frac{K_2\Delta E - k'^2\Delta\Pi}{v_m K_1 k} \right) \tag{3.33}$$

Here ΔE and $\Delta\Pi$ are the difference between the incomplete and the complete elliptic integrals of the second and thirds kinds,

$$\Delta E = E(\phi, k) - E(k), \quad \Delta\Pi = \Pi(n;\phi,k) - \Pi(n;k)$$

Their arguments, modulus, and parameter are:

$$\sin\phi = \frac{v_m}{v}\sqrt{\frac{2}{1+\sin\psi}}, \quad k = \sqrt{\frac{1-K_2}{2}}, \quad n = \frac{K_2 - 1}{2K_2}$$

and k' is the complementary modulus, which relates to the modulus k by $k^2 + k'^2 = 1$ and thus being:

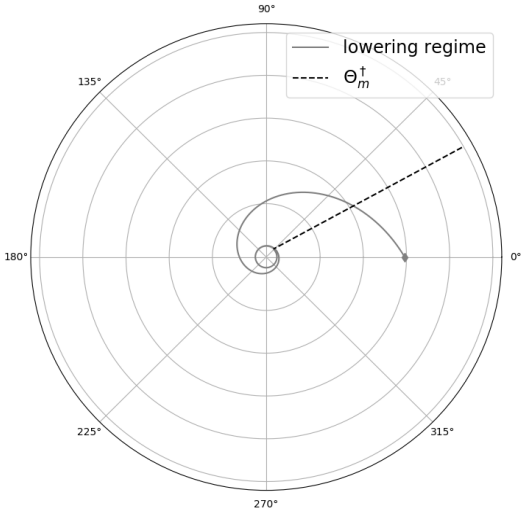

Figure 3.5: A lowering elliptic spiral departing from $\diamond$.

$$k' = \sqrt{\frac{1+K_2}{2}}$$

The time equation 3.33 resembles Kepler's equation, provided that t_m can be seen as the spiral equivalent to the time of periapsis passage. t_m is solved from the initial conditions r_0, t_0 in equation 3.33:

$$t_m = t_0 \mp \left(\frac{r_0 v_0}{K_1} \sqrt{\frac{1-\sin\psi_0}{1+\sin\psi_0}} + \frac{K_2 \Delta E_0 - k'^2 \Delta \Pi_0}{v_m K_1 k} \right) \tag{3.34}$$

The sign corresponds to raising/lowering regime accordingly.
The time of flight to describe the generating spiral,t_Γ is:

$$t_\Gamma = \frac{2\left[K_2 E(k) - k'^2 \Pi(n;k)\right]}{v_m K_1 k} \tag{3.35}$$

Note that $t_\Gamma = f(K_1, K_2)$, so it is a unique value for each elliptic spiral defined. It represents the maximum time that any elliptic spiral will need to connect two points.

3.4 Parabolic Spirals

This type of spirals are the equivalent to the logarithmic spirals. Because $K_1 = 0$ equation 3.16 yields:

$$v^2 = \frac{1}{r} \longrightarrow v = \frac{1}{\sqrt{r}} \tag{3.36}$$

In other words, the velocity coincides with the local circular velocity. Contrary to elliptic spirals, parabolic spirals trajectory, if in raising regime, can keep increasing without any restriction, so they can hypothetically reach infinity ($r \to \infty$). It is interesting to study the velocity these spirals reach infinity with. Taking limits and using equation 3.36:

$$\lim_{r\to\infty} v = 0$$

This results shows that parabolic spirals reach infinity with zero velocity, just like parabolic orbits in the Keplerian case.

Another characteristic of these spirals worth studying, is the flight-direction angle ψ. For $K_1 = 0$, from equation 3.21 is easy to see that the evolution of ψ with the trajectory ($d\psi/dr$) becomes zero. Therefore, ψ must be constant along the trajectory of parabolic spirals. To obtain the value of ψ, equation 3.16 can be introduced in equation 3.19, yielding:

$$\sin\psi = K_2, \quad \text{and} \quad \cos\psi = \pm\sqrt{1 - K_2^2} = \pm l \tag{3.37}$$

In the limit case $\psi = \pi/2 \to K_2 = 1$ parabolic spirals degenerate into circular Keplerian orbits. The thrust vanishes and, since ψ is constant, it will remain zero. Also, equation 3.37a shows that K_2 is restricted to the interval $K_2 \in (0, 1]$ because of the sin function.

The trajectory

Parabolic spirals have been compared with logarithmic spirals. Thus, when solving the equations of motion (3.11-3.14) for $K_1 = 0$, solution must match with the equations from logarithmic spirals.

Starting with θ, equation 3.23 is integrated to provide:

$$\theta - \theta_0 = \pm\frac{K_2}{l}\ln\left(\frac{r}{r_0}\right) \tag{3.38}$$

Taking limits to equation 3.38: $\lim_{r\to\infty}\theta(r) = \infty$ which shows that the particle follows a spiral branch when reaching infinity.

To obtain the trajectory, equation 3.38 have to be inverted:

$$r(\theta) = r_0 e^{(\theta-\theta_0)\cot\psi} \tag{3.39}$$

which is the equation of a logarithmic spiral.

Evangelista Torricelli, back in the 17th century, was the first to be able to integrate the length of a logarithmic spiral. Therefore, the arclength of the logarithmic spiral can be measured by Torricelli expresion:

$$s(\theta) = \frac{r_0}{\cos\psi}\left[e^{(\theta-\theta_0)\cot\psi} - 1\right] \tag{3.40}$$

Figure 3.6 represents two parabolic spirals with an initial flight-direction angle $\psi = 88°$. Although both spirals start from the same place and have the same initial conditions $(r_0, v_0, \theta_0, \psi_0, t_0)$, their trajectories differ due to one being in raising regime while the other one is in lowering regime.

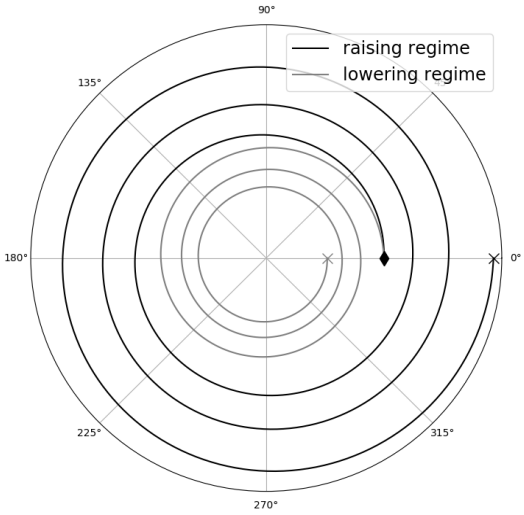

Figure 3.6: Pair of parabolic spirals in different regimes, for $\psi = 88°$. The spiral start at $\diamond$ and end at $\times$.

The time of flight

The time of flight can be solved from the inverse of the radial velocity, yielding:

$$t = t_0 \pm \frac{2}{3l}\left(r^{3/2} - r_0^{3/2}\right) \tag{3.41}$$

Taking limits in this last equation 3.41: $\lim_{r\to\infty} t(r) = \infty$, which means that it takes an infinite time to reach infinity. This result match perfectly with the velocity one. Because a parabolic spiral reach infinity with a velocity of zero, takes it an infinite time to reach infinity.

On the other hand, studying parabolic spirals in lowering regime:

$$\lim_{r\to 0} t(r) = \frac{2r_0^{3/2}}{3l}$$

which is the time needed to reach the center. However, note that for a flight angle $\psi = \pi/2 \to l = 0$, so the time to reach the center becomes zero. This means that the spiral never reach the origin because the spiral degenerate into a circular Keplerian orbit.

3.5 Hyperbolic Spirals

Hyperbolic spirals are defined by a positive constant of the generalized energy. If these spirals are in raising regime, they reach infinity with a finite, nonzero velocity. This velocity can be calculated from equation 3.16:

$$v_\infty = \lim_{r\to\infty} \sqrt{K_1 + \frac{1}{r}} = \sqrt{K_1} \longrightarrow K_1 \equiv C_3 \tag{3.42}$$

This result is analogous to the Keplerian case, where the hyperbolic excess velocity is defined by the characteristic energy, $C_3 = v_\infty^2$.

Studying the flight-direction angle ψ, from equation 3.21 is easy to see that, for these spirals with positive generalized energy, ψ always decreases along hyperbolic spirals.

Parabolic spirals could reach infinity as well, but whereas parabolic spirals did it along a spiral branch, hyperbolic spirals reach infinity along an asymptotic branch. In the limit case $r \to \infty$ the polar angle θ converges to a finite value θ_{as}. Its value will be calculated later in this chapter. Because ψ decreases with time, the position and velocity vector will become parallel at infinity. The impact parameter of the resulting asymptotes,c, can be solved from the equation of the angular momentum, 3.18:

$$h = v_\infty c \longrightarrow c = \frac{K_2}{K_1} \tag{3.43}$$

What really this parameter c defines is the minimum distance from the asymptote to the center of attraction.

A very special characteristic of these spirals is the distinction of two subfamilies of hyperbolic spirals. The distinction attends to the values K_2 can take, as it is going to be shown.

Equation 3.20 is correct for all generalized logarithmic spirals. It relates K_1 and K_2 with ψ. Of course the term $\sin\psi$ is bounded to $\sin\psi \leq 1$. For $K_2 \leq 1$ this condition is satisfied naturally, provided that $K_1 r \geq 0$. However, if $K_1 > 1$ this condition only holds if

$$r \geq r_{min} = \frac{K_2 - 1}{K_1}$$

This proves that a minimum radius exists for hyperbolic spirals with $K_2 \geq 1$, so they will never reach the center of attraction because they cannot travel further than this boundary r_{min}. The minimum radius is referred to as the periapsis of the spiral. Another analogy can be made, recalling equation 3.26 which describes the value of the maximum radius of an elliptic spiral. Both expressions, r_{min} and r_{max} are identical, the only difference between them is the values K_1 and K_2 actually take for each type of spiral.

Going back to the two hyperbolic subfamilies, it has been made clear that a notable difference exists: a subfamily with $K_2 < 1$ (hyperbolic spirals Type I) which have no limits to the values their radius can take, and a subfamily with $K_2 > 1$ bounded to a minimum radius.

Also, as it will be shown later in this section, they also have another difference. Type I hyperbolic spirals have only one asymptote, whereas Type II hyperbolic spirals have two asymptotes.

Note that the case where $K_2 = 1$ has not been mentioned. This is because the limit $K_2 \to 1$ defines the transition between the two subfamilies, Type I and Type II hyperbolic spirals, but it is not considered as an own subclass of the hyperbolic spirals family.

Type I hyperbolic spirals

These spirals are defined by $K_1 \in (0, \infty)$ and $K_2 \in (0, 1)$. As it was proved before, the condition $\sin\psi \leq 1$ equation 3.20 imposes holds naturally and so, the radius has no limitations in the values it can take. In order to study the dynamics of the particle when reaching the origin it is necessary to take limits in equation 3.20:

$$\lim r \to 0 \psi(r) = \pi - \arcsin K_2$$

Since $K_2 < 1 \longrightarrow K_2 < \pi/2$, which means that ψ will never cross $\psi = \pi/2$. In other words, the trajectory remains in lowering regime.

On the other hand, if initially $\psi_0 < \pi/2$ then the spiral will be in raising regime forever. The asymptotic escape is defined by $\lim r \to \infty \psi(r) = 0$, which translates in a position and velocity vectors parallel to each other. Since the flight direction angle always decreases, it is not possible for the trajectory to transition to lowering regime.

Overall, a body in lowering regime will always fall to the center of attraction, whereas a body in raising regime will always escape to infinity. Natural transitions between regimes are not possible since $\cos\psi$ can never change its sign.

The trajectory

Integrating equation 3.27 for $K_2 < 1$:

$$\theta - \theta_0 = \pm\frac{K_2}{l}\ln\left[\frac{r\sin\psi}{r_0\sin\psi_0}\left(\frac{1 - K_2\sin\psi_0 + l|\cos\psi_0|}{1 - K_2\sin\psi + l|\cos\psi|}\right)\right] \tag{3.44}$$

Is easy to see that there are two possible solutions, depending the choice of the $\pm$ sign. If limits to this equation are taken, then the direction to the asymptote θ_{as} can be calculated, $\theta_{as} = \lim_{r\to\infty}\theta(r)$:

$$\theta_{as} = \theta_0 + \frac{K_2}{l}\ln\left[\frac{K_2(l|\cos\psi_0| + 1 - K_2\sin\psi_0)}{(K_2 - \sin\psi_0)(1 + l)}\right] \tag{3.45}$$

$$\theta^{\dagger}_{as} = \theta_0 - \frac{K_2}{l}\ln\left[\frac{K_2(l|\cos\psi_0| + 1 - K_2\sin\psi_0)}{(K_2 - \sin\psi_0)(1 + l)}\right] \tag{3.46}$$

Equation 3.45 is valid for raising regime spirals whereas 3.46 is valid for lowering regime spirals.

The equation for the trajectory is obtained upon inversion of equation 3.44 and introducing the direction of the asymptote:

$$r(\theta) = \frac{l^2/K_1}{2\sinh\frac{\beta}{2}\left(\sinh\frac{\beta}{2} + l\cosh\frac{\beta}{2}\right)} \tag{3.47}$$

where

$$\beta = \frac{l}{K_2}(\theta_{as} - \theta), \qquad \beta^{\dagger} = -\frac{l}{K_2}(\theta^{\dagger}_{as} - \theta)$$

As always, β is for raising regime spirals and $\beta^{\dagger}$ is for lowering regime spirals. Is the direction of the initial velocity what determines which one to choose.

The asymptotes θ_{as} and $\theta^{\dagger}_{as}$ intersect on the axis of symmetry at a distance d from the center of attraction. This distance can be calculated with the impact parameter equation 3.43 it was introduced earlier:

$$d = \frac{K_2}{K_1|\sin(\theta_{as} - \theta_0)|} = \frac{K_2}{K_1|\sin(\theta^{\dagger}_{as} - \theta_0)|}$$

Figure 3.7 sums up everything studied about the trajectory of hyperbolic type I spirals. It pictures two hyperbolic type I spirals, one in raising regime and the other in lowering regime. Asymptotes from each spiral are also pictured, and they intersect with each other in a point at a distance d from the center of attraction.

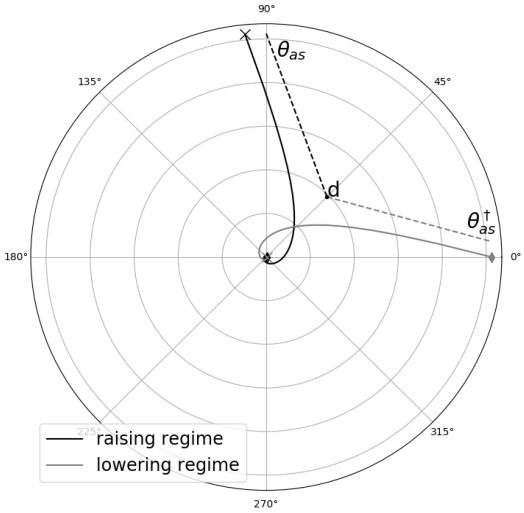

Figure 3.7: Two hyperbolic Type I spirals. The spirals start at $\diamond$ and end at $\times$.

The time of flight

Integrating equation 3.32 for $K_2 < 1$ requires the use of the incomplete elliptic integrals of the second and third kinds, $E = E(\phi, k)$ and $\Pi = \Pi(n; \phi, k)$, respectively:

$$t(r) = K_4 \pm \left(\frac{rv}{K_1} \sqrt{\frac{1+\sin\psi}{1-\sin\psi}} - \frac{K_2 E + k'^2 \Pi}{K_1 \sqrt{K_1 K_2/2}} \right) \tag{3.48}$$

where

$$\sin\psi = \sqrt{\frac{2rK_1 \sin\psi}{(1+K_2)(1-\sin\psi)}} \quad k = \sqrt{\frac{1+K_2}{2}}, \quad k' = \sqrt{\frac{1-K_2}{2}} \quad n = \frac{1+K_2}{2K_2}$$

Note that k and k' are complementary. This is, $k^2 + k'^2 = 1$. The constant of integration K_4 is obtained from the initial conditions as follows:

$$K_4 = t_0 \mp \left(\frac{r_0 v_0}{K_1} \sqrt{\frac{1+\sin\psi_0}{1-\sin\psi_0}} - \frac{K_2 E_0 + k'^2 \Pi_0}{K_1 \sqrt{K_1 K_2/2}} \right) \tag{3.49}$$

where $E_0 = E(\phi_0, k)$ and $\Pi_0 = \Pi(n; \phi_0, k)$

The time to reach the origin derives from the limit $\lim_{r\to 0} t(r) = K_4$. It is a finite time and depends on the initial conditions following equation 3.49.

Type II hyperbolic spirals

These spirals are defined by $K_1 \in (0, \infty)$ and $K_2 \in (1, \infty)$. As it was proven before in this section, a particle moving along a Type II hyperbolic spiral, if in lowering regime, will reach a limit radius r_{min} when $\psi = \pi/2$. Then, it will transition into raising regime and escapes to infinity.

Therefore, it will never reach the origin. Once the particle is in raising regime, because of the positive generalized energy that makes ψ always decrease, it will stay forever in this regime and it will escape to infinity.

It is safe to say that a Type II hyperbolic spiral can only be in lowering regime if it was initially in lowering regime. If the particle initially is in $r_0 = r_{min}$ the spiral immediately transitions to raising regime and escapes to infinity. Figure 3.9 depicts precisely the natural transition from lowering to raising regime of these spirals.

The velocity of the particle when reaching the minimum radius (periapsis) is obtained from equation 3.16:

$$v_{max} = \sqrt{\frac{K_1 K_2}{K_2 - 1}} = \sqrt{\frac{K_2}{r_{min}}} \tag{3.50}$$

Note that this expression, and the way it was obtained, is analogous with the elliptic case, see equation 3.25

The trajectory

The evolution of the polar angle for Type II hyperbolic spirals is found solving equation 3.27 for $K_2 > 1$:

$$\theta - \theta_m = \pm \frac{K_2}{l} \left\{ \frac{\pi}{2} + \arctan \left[\frac{1 + K_1 r - K_2^2}{l\sqrt{(1+K_1 r)^2 - K_2^2}} \right] \right\} \tag{3.51}$$

where $l = \sqrt{(K_2^2 - 1)}$.

θ_m is obtained from the initial conditions (r_0, θ_0):

$$\theta_m = \theta_0 - \frac{K_2}{l}\left\{\frac{\pi}{2} + \arctan\left[\frac{1 + K_1 r_0 - K_2^2}{l\sqrt{(1 + K_1 r_0)^2 - K_2^2}}\right]\right\} \tag{3.52}$$

$$\theta_m^\dagger = \theta_0 + \frac{K_2}{l}\left\{\frac{\pi}{2} + \arctan\left[\frac{1 + K_1 r_0 - K_2^2}{l\sqrt{(1 + K_1 r_0)^2 - K_2^2}}\right]\right\} \tag{3.53}$$

As always, two different trajectories emanate from these equations. Equation 3.52 is valid for raising regime and equation 3.53 is valid for lowering regime. The choice is determined by the direction of the initial velocity vector $\mathbf{v}_0$.

For the trajectory equation, solving equation 3.51 for the radius:

$$r(\theta) = r_{min}\frac{1 + K_2}{1 + K_2 \cosh\beta} \tag{3.54}$$

where the spiral anomaly β can take the following expressions:

$$\beta = \frac{l}{K_2}(\theta - \theta_m), \qquad \beta^\dagger = \frac{l}{K_2}(\theta - \theta_m^\dagger)$$

depending if the spiral is in raising or lowering regime, respectively.

Type II hyperbolic spirals in lowering regime will always intersect themselves at least once, if they have adequate initial conditions and sufficient revolutions for the intersection to happen. Intersection occur on the axis of symmetry $\theta = \theta_m$.

However, if they are in raising regime, they will reach infinity as it was proved before. The conditions of the spiral to reach infinity can be studied from the limit $r \to \infty$. The existence of two asymptotes for these Type II hyperbolic spirals can be proved from equation 3.54: the denominator cancels for

$$\beta = \pm\arccos\left(-\frac{1}{K_2}\right) \longrightarrow \theta_{as}^{\pm} = \theta_m \pm \frac{K_2}{l}\arccos\left(-\frac{1}{K_2}\right)$$

This equation defines the orientation of the two asymptotes for a raising regime, symmetric with respec to to θ_m. The two asymptotes corresponding lowering regime can be calculated as follows:

$$\theta_{as}^{\pm\,\dagger} = \theta_m^\dagger \pm \frac{K_2}{l}\arccos\left(-\frac{1}{K_2}\right)$$

The difference between the asymptotes $\theta_{as}^{\pm}$ and $\theta_{as}^{\pm\,\dagger}$ comes from the fact $\theta_{as}^{\pm} \neq \theta_{as}^{\pm\,\dagger}$

Figures 3.8 and 3.9 depict two hyperbolic Type II spirals. They have been obtained by the use of the equations just obtained.

Note the natural transition between lowering/raising regime as well as the self-intersection in 3.9. Also note how θ_m happens to be the axis of symmetry, and the two asymptotes that differentiates this Type II hyperbolic spirals with the Type I hyperbolic spirals which only had one asymptote.

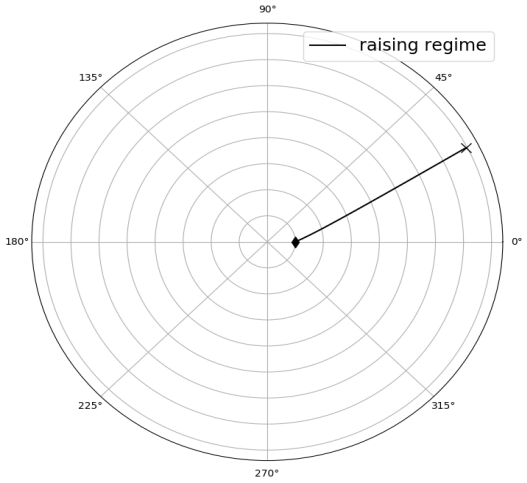

Figure 3.8: Hyperbolic spiral Type II in raising regime. The spiral starts at $\diamond$ and ends at $\times$.

The time of flight

Integrating equation 3.32 and introducing the time of periapsis passage t_m, the time of flight reads:

$$t(r) - t_m = \pm \frac{1}{K_1^{3/2}} \left\{ \sqrt{\frac{z(z^2 - K_2^2)}{(z-1)}} - \arcsin \sqrt{\frac{(z-1)(z-K_2)}{z + K_2(2z-1)}} + \frac{\sqrt{2}[k'^2(\Pi + K_2 F) - K_2 E]}{k\sqrt{K_2}} \right\} \quad (3.55)$$

where $z = 1 + K_1 r$. The arguments of the elliptic integrals are:

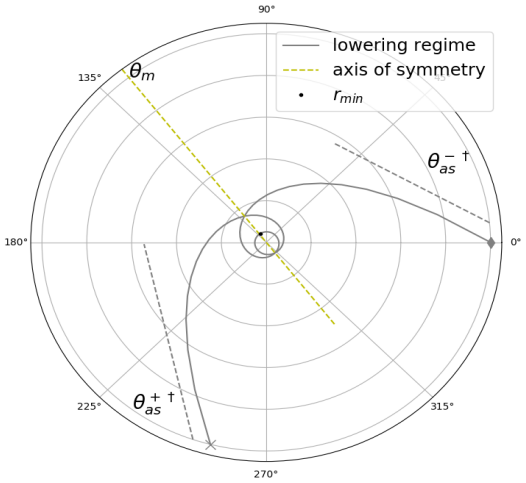

Figure 3.9: Hyperbolic spiral Type II in lowering regime. The spiral starts at ⋄ and ends at ×.

$$\sin\phi = \sqrt{\frac{n(z-K_2)}{k^2(z-1)}}, \quad k = \sqrt{\frac{2}{1+K_2}}, \quad k' = \sqrt{\frac{K_2-1}{K_2+1}}, \quad n = \frac{1}{K_2} \tag{3.56}$$

The time of flight to the periapsis, t_m can be calculated from equation 3.55 for $r = r_0$:

$$t_m = t_0 \mp \frac{1}{K_1^{3/2}} \left\{ \sqrt{\frac{z_0(z_0^2-K_2^2)}{(z_0-1)}} - \arcsin\sqrt{\frac{(z_0-1)(z_0-K_2)}{z_0+K_2(2z_0-1)}} + \frac{\sqrt{2}[k'^2(\Pi_0+K_2F_0)-K_2E_0]}{k\sqrt{K_2}} \right\} \tag{3.57}$$

3.6 Summary

After discussing all three families that compose the generalized logarithmic spirals, it is useful to sum all that up in the next table:

Type of spiral	K_1	K_2	Trajectory	TOF
Elliptic	< 0	$\in (0, 1)$	Eq.3.31	Eq.3.33
Parabolic	$= 0$	$\in (0, 1]$	Eq.3.39	Eq.3.41
Hyperb. Type I	> 0	$\in (0, 1)$	Eq.3.47	Eq.3.48
Hyperb. Type II	> 0	> 1	Eq. 3.54	Eq.3.55

Table 3.1: Conditions and main equations for the different families of the generalized logarithmic spirals.

3.7 Conclusions

In this chapter the entire generalized logarithmic spirals family was presented, showing that a not-rigorous approach misses an entire family of solutions. During the chapter, multiple similarities and analogies with the Keplerian case were pointed out. Three different families were found: elliptic, parabolic and hyperbolic, where parabolic spirals turned out to be logarithmic spirals. Also for the same family spiral, two regimes could be taken depending on the initial velocity vector of the particle. The generalized logarithmic spirals theory is purely dynamical, meaning that all the parameters have a physical interpretation (for example K_1 represents the Keplerian energy, K_2 represent the angular momentum...) which proves useful and handy when operating with this generalized solution. Also, because the constant flight-direction angle in parabolic spirals, they are less interesting in mission design because its lower flexibility and options. Elliptic and hyperbolic spirals are usually of more interest, specially the elliptic spirals when treating with low-thrust trajectory design.

Chapter 4

Implementation and Validation

"If things are not failing, you are not innovating enough"
-Elon Musk

HAVING obtained the analytic solution that yielded the generalized logarithmic spirals theory, it is time to implement all of this work in a code. This code should be able to, for a given spiral, classify it into the three families there are, calculate the parameters that define the spiral and solve the trajectory and time of flight equations of the spiral.

After that, a validation phase will be mandatory in order to verify if there was any unintentional mistake during the code writing and to proof that the analytic solution was solved correctly in chapter 3.

Although validation and software debugging is many times a hard bone, one could not trust his results without this step. Therefore, it is usually one of the most time consuming phases of writing code, and one of the most important phases as well.

In the following chapter the implementation scheme will be briefly explained. Then, the methods used for the validation of the code will be mentioned and explained. Lastly, the results of these stages (mainly a comparison between the numerical solution and the analytic solution of the problem) will be shown.

4.1 Implementation

In chapter 3 rather long and complicated expressions where obtained from the analytic solution. In order to operate and solve these equations, the programming language Python will be used. Python is an interpreted high-level programming language for general-purpose programming. It is object-oriented, an important characteristic for the implementation scheme followed in this thesis.

Generalized logarithmic spirals are divided in three families of spirals: elliptic, parabolic and hyperbolic. Therefore, a base class **class** *Logspiral* has been created. This fulfills two purposes: firstly, to initialize a spiral and to determine the family it belongs to; and secondly, to gather all the common characteristics and equations of the generalized logarithmic spirals, such as the basic initial conditions $(r_0, v_0, \theta_0, \psi_0, t_0)$ or constants K_1, K_2, K_3, K_4. Also, four derived classes:

class *Ellspiral(Logspiral)*,

class *Parspiral(Logspiral)*,

class *HypspiralI(Logspiral)*,

class *HypspiralII(Logspiral)*

have been created, one for each family/subfamily of the generalized logarithmic spirals. Each of them has its own methods for the different equations and parameters of its family. To be able to find the family any given spiral belongs to, it has been implemented a function called *findspiraltype* that, from the constants K_1 and K_2, distinguish between these families and change the type of spiral accordingly. For example, a spiral could be defined as *examplespiral = Logspiral(K1=-0.01,K2= 0.8,...)* and then the code identify the family it belongs to and change the type to, in this case, elliptic. From here, all the equations and parameters calculated will belong to the elliptic case.

The code has been designed to be as flexible as possible. For example, four different sets of inputs can be used to initialize any given spiral:

'K' initialization: this initialization takes as arguments the four constants that define completely a spiral by its shape (K_1, K_2), orientation (K_3) and time reference K_4, in addition to the regimen the spiral is in ($'raising'$ or $'lowering'$) and its initial distance to the center of attraction (r_0). With this, it is able to calculate the initial conditions of the particle, its trajectory, the time of flight...

'initial conditions': it passes the initial conditions $r_0, v_0, \theta_0, \psi_0, t_0$ and the spiral regime ($'raising'$ or $'lowering'$). With these data, it can obtain the four constants and distinguish the type of the spiral.

'vector': it is possible to have as input the position and velocity vector of the particle, in addition to the initial time t_0, from where the code is able to calculate the initial conditions $r_0, v_0, \theta_0, \psi_0$ and similarly to the previous initialization, calculate from them the constant values.

'components': this initialization works with the components of the position and velocity vectors of the particle. It is very similar to the 'vector' initialization, but passing the components of the vector instead of the vector itself.

Each of the procedures above, before and after finding the type of the spiral, check the values of the constants and initial variables to make sure the spiral introduced physically exists. They make sure that the spiral parameters do not exceed their boundaries, if they have any, or that they do not produce a $\sin\psi > 1$ for example- If an error of this kind is found, the code raises an exception indicating the problem and terminates the program.

Another effort for the sake of code flexibility has also been implemented. To calculate the trajectory, or the time of flight, or any wanted equation, both single values and lists of values are accepted.

Lastly, plots methods for each type of spiral have been included to facilitate this routinary action. With two options of plotting, in a single graph or in the same graph (useful when comparing spirals), the trajectories $r(\theta)$ of the spirals can be obtained. In addition to the trajectory, characteristic features of each type of spiral are also plotted (such as symmetries, asymptotes or maximum and minimum radius). This methods have proven very useful during the thesis.

4.2 Numeric and Analytic Solution

The dynamic of a particle under the action of a central gravitational force and a perturbing acceleration can be described with the differential equation 3.1. Therefore, an expression $r(t)$ could be obtained by integrating this differential equation. In order to solve the differential equation, the following steps have been carried out. First, because it is a second order differential equation, it must be broken down into two first order differential equations:

$$\frac{d^2\mathbf{r}}{dt^2} + \frac{\mu}{r^3}\mathbf{r} = \frac{\mu}{2r^2}\cos\psi\mathbf{t} \longrightarrow$$
$$\overset{\text{new variable}}{\longrightarrow} \frac{d\mathbf{r}}{dt} = \mathbf{v}$$
$$\frac{d\mathbf{v}}{dt} = \frac{\mu}{2r^2}\cos\psi\mathbf{t} - \frac{\mu}{r^3}\mathbf{r}$$

Now, the problem can be converted to cartesian coordinates through the following identities:

$$\mathbf{r} = \begin{bmatrix}\mathbf{x}\\ \mathbf{y}\end{bmatrix},\ \mathbf{v} = \begin{bmatrix}\dot{\mathbf{x}}\\ \dot{\mathbf{y}}\end{bmatrix},\ r = \sqrt{x^2+y^2},\ v = \sqrt{\dot{x}^2+\dot{y}^2}$$
$$\mathbf{t} = \frac{\mathbf{v}}{v} = \frac{1}{\sqrt{\dot{x}^2+\dot{y}^2}}\begin{bmatrix}\dot{\mathbf{x}}\\ \dot{\mathbf{y}}\end{bmatrix},\ \cos\psi = \frac{\mathbf{r}\cdot\mathbf{v}}{rv}$$

The coordinate change has increased the number of differential equations, due to $\mathbf{r}$ and $\mathbf{v}$ being expressed by two cartesian coordinates each. In order to write the above in the state-space $\rightarrow x = X_1$, $y = X_2$, $\dot{x} = X_3$, $\dot{y} = X_4$ and so,

$$\dot{X}_1 = X_3$$
$$\dot{X}_2 = X_4$$
$$\dot{X}_3 = \frac{\mu}{2r^2}\cos\psi X_3 - \frac{\mu}{r^3}X_1$$
$$\dot{X}_4 = \frac{\mu}{2r^2}\cos\psi X_4 - \frac{\mu}{r^3}X_2$$

Notice that the first two equations correspond to the first differential equation $d\mathbf{r}/dt$ and the last two equations correspond to the second differential equation $d\mathbf{v}/dt$. The state-space is as follows:

$$\dot{X} = \begin{bmatrix}\dot{X}_1\\ \dot{X}_2\\ \dot{X}_3\\ \dot{X}_4\end{bmatrix} = \underbrace{\begin{bmatrix} 0 & 0 & 1 & 0\\ 0 & 0 & 0 & 1\\ -\frac{\mu}{r^3} & 0 & \frac{\mu}{2r^2}\cos\psi & 0\\ 0 & -\frac{\mu}{r^3} & 0 & \frac{\mu}{2r^2}\cos\psi\end{bmatrix}}_{A}\underbrace{\begin{bmatrix}X_1\\ X_2\\ X_3\\ X_4\end{bmatrix}}_{X}$$

After these transformations, the differential equation is solved with the python method *odeint* from the package *integrate*.

On the other hand, from the analytic study, the trajectory $r(\theta)$ and the time of flight $t(r)$ equations were obtained, among other equations. Therefore, to proof the analytic solution (which was obtained from the differential equation) and to check that no mistypes were made, both solutions, numeric and analytic, should match when compared to each other under the same conditions.

In order to do so, for a common time interval $t = (t_0, t_f, step)$, equation 3.1 must be integrated, and its correspondent analytic solution must be solved, obtaining in result the same values of r for the same period of time.

A problem is faced in this stage. The differential equation yields a $r(t)$ expression whereas the analytic approach yields a $t(r)$ expression. In a lot of equations this would not be a huge problem because inverting the $t(r)$ expression is usually not complicated. But as it was mentioned in subsection 3.2, similarly to Kepler's equation, the equation of time of flight cannot be inverted analytically, so it must be inverted numerically. Nevertheless, the parabolic time of flight equation is an exception because it can be inverted analytically, so this will be taken advantage of.

To numerically invert the time of flight equation, $t(r) \longrightarrow r(t)$, a root-finding algorithm has been used as follows. The expression $t(r)$ is known, therefore for any given value $r^* \rightarrow t(r^*) = t^*$ the corresponding time to that distance is known. The problem of inverting this equation can be seen as, what is the value of r that satisfies $t(r) = t^*$?, or equivalently, $t(r) - t^* = 0$. This function $F = t(r) - t^* = 0$ is the one the root-finding algorithm is going to be applied to. For every point of the function $r(t^*)$ that needs to be calculated, the root of the function $F = t(r) - t^*$ needs to be found.

Now, there are many root-finding algorithms, each one with advantages and disadvantages. Firstly, Newton-Raphson algorithm was considered, because it has one of the fastest convergences (it converges quadratically) and it is easy to implement. The derivative of the function F was numerically calculated. But this method was not perfectly suited for our specific case. In figure 4.1 the form of the function F is shown. Because it is an elliptic spiral, its radius is limited to r_{max}. Not only that, once it reaches it, the spiral radius starts to decrease, resulting in that graph.

When applying Newton, the region of the domain of the graph became a problem. In the process of finding the root, it jumped to values of r out of the domain of the graph, so an error raised. So an alternative root-finding algorithm was needed, one with restrictions in the domain of the graph. The bisect method was chosen. Although slower than Newton, it was better suited for this case. It needs two points (with different sign) to begin, and it never leaves that interval of values. Despite the convergence velocity, another disadvantage of the method is the impossibility of finding

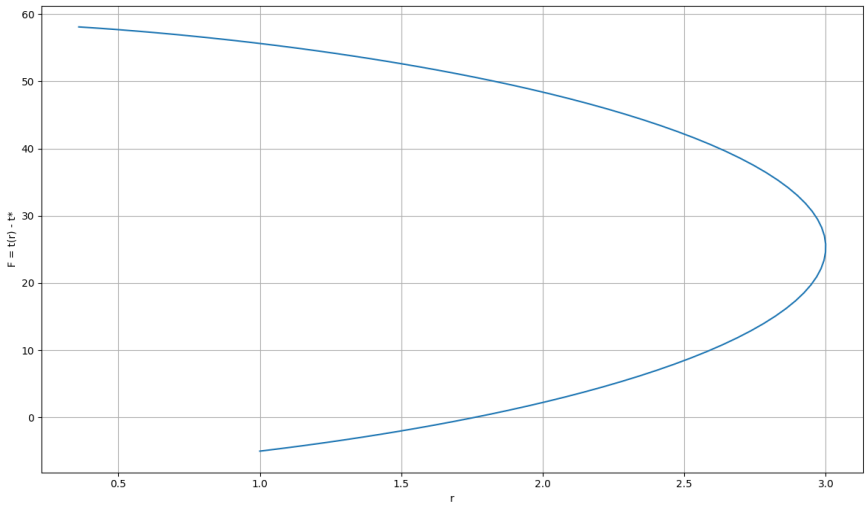

Figure 4.1: $F = t(r) - t^*$ for an elliptic spiral with $t^* = 5$

multiple roots. Luckily, the function F just have one. The last problem was the tricky shape of the graph. Because the radius increased and decreased, the same interval that worked for the 'raising region' did not work for the 'lowering region'. Thus, a variable interval had to be implemented. So for t^* values smaller than t_m (recall that t_m was the time needed to reach r_{max}) the interval $[r_0, r_max]$ was chosen, and when evaluating t^* greater than t_m (which translates in a decreasing radius), the interval $[r_max, r[-1]$ was chosen. $r[-1]$ refers to the last plotted point of r.

Finally, both numeric and analytic $r(t)$ equations were obtained.

4.3 Validation

The error between the numeric and the analytic solutions will be measured in terms of the difference in the trajectory of each solution for the same period of time. Therefore, the error will be calculated as:

$$error = \left| \frac{r_{numeric} - r_{analytic}}{r_{numeric}} \right| \tag{4.1}$$

The difference between trajectories has been divided by one of the trajectories to obtain a dimensionless error. In addition, the error will be represented in a logarithmic scale.

The following figures represent the error over time of the different generalized logarithmic spirals families.

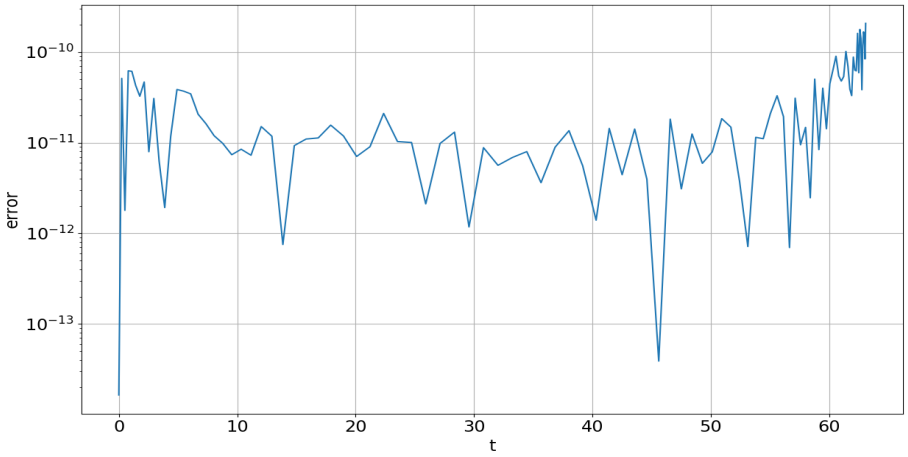

Figure 4.2: Dimensionless error over time for the analytic solution of a generalized elliptic spiral.

Figure 4.2 depicts the error for an elliptic spiral. Initially in raising regime, during the integration time the spiral reached r_{max} to then transition into lowering regime until reaching the center. The error is bounded up to $1e^{-10}$, with a mean error of approximately $1e^{-11}$. The error has not been affected by the regime transition.

Figure 4.3 depicts the error for a parabolic spiral in raising regime. Note that for low integration times the error is on the order of $1e^{-12}$, but as time progresses the error grows slowly but surely. This is because these type of spirals are not limited by their radius, so as the radius grows exponentially, the analytic solution differ a little bit more each time respect to the numeric solution. Still, the error is acceptable, with a mean error value of not even $1e^{-11}$.

Figure 4.4 depicts the error for an hyperbolic Type I spiral in raising regime. This graph soon reaches a steady error on the order of $1e^{-11}$ that maintains during all the integration time.

Figure 4.5 depicts the error for an hyperbolic Type II spiral initially in lowering regime. As it was already explained in chapter 3, these types of spiral when in lowering regime transitions to raising regime and so this configuration has been chosen in order to see if the transition affect the error in any way. Similarly to the elliptic case, it did not. The spiral transitions very quickly to raising regime because the initial radius r_0 given

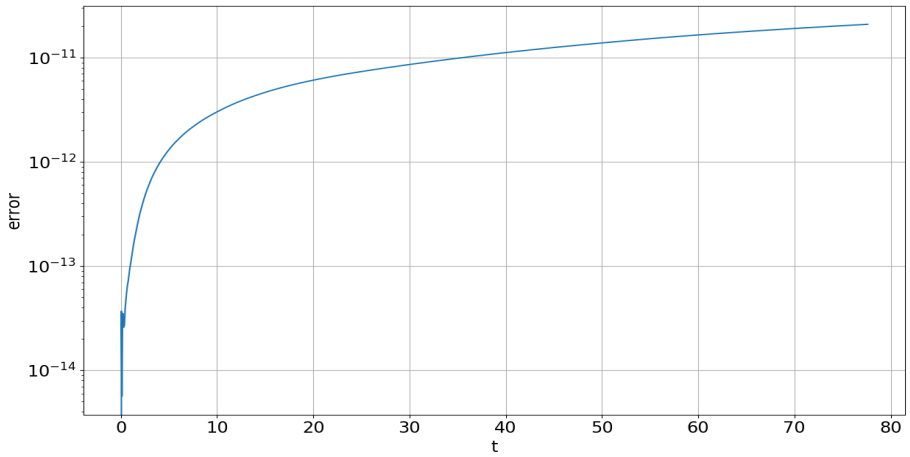

Figure 4.3: Dimensionless error over time for the analytic solution of a generalized parabolic spiral.

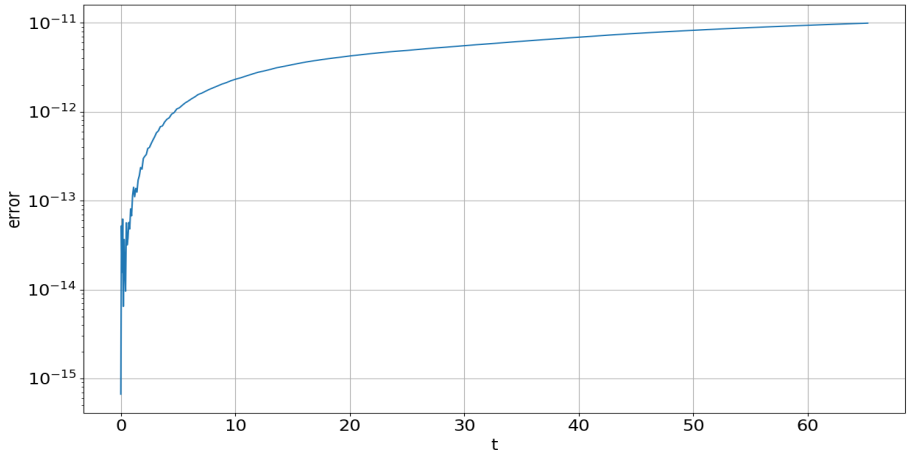

Figure 4.4: Dimensionless error over time for the analytic solution of a generalized hyperbolic Type I spiral.

was very close to the minimum radius of the spiral. Note that similarly to the parabolic example, once in raising regime it is able to reach infinity, and so, as the radius grows really fast, the error between the analytic and the numeric solution slowly grows.

Finally, note that the mean error order for all four types of spirals is

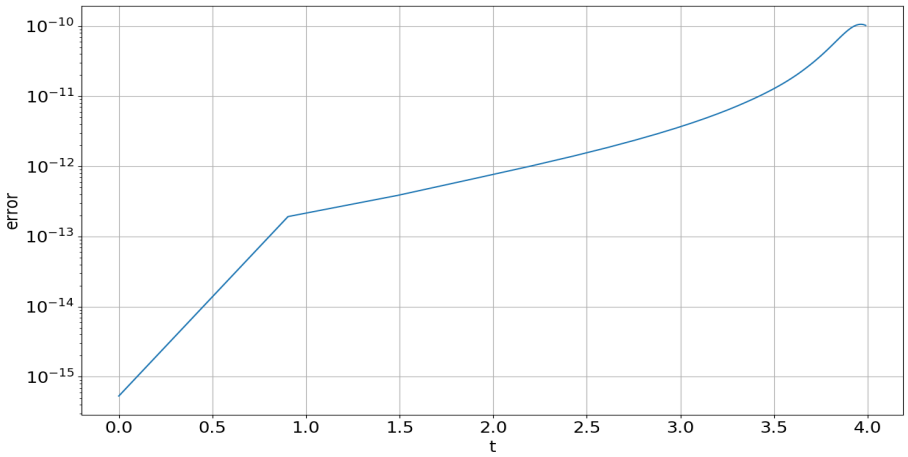

Figure 4.5: Dimensionless error over time for the analytic solution of a generalized hyperbolic Type II spiral.

about $1e^{-11}$. It is not a coincide as it is related to the tolerance chosen to solve the differential equation 3.1. For these particular examples, a tolerance of $1e^{-12}$ was chosen.

4.4 Conclusions

After having a look at the errors between the numeric and the analytic solution, it is safe to say that the analytic problem was solved accurately, and the equations of chapter 3 describe precisely the motion of a particle under a gravitational and a perturbing acceleration.

Also, the excellent results obtained in the chapter are a solid proof that the equations were implemented correctly and that the code works.

Chapter 5

Lambert´s problem

Mathematics is the queen of sciences.
She often condescends to render service
to astronomy and other natural sciences,
but in all relations she is entitled to the first rank.
-Carl Friedrich Gauss

REACHING an asteroid, or any space object by the same means, reduces to finding the orbit that connects two position vectors in a certain time. The Swiss scientist Johann Heinrich Lambert was the pioneer in addressing this problem, and so the problem is usually referred to as the Lambert's problem. A big contribution to this particular problem was made by no other than Carl Friedrich Gauss, popularly known as The Prince of Mathematicians. Gauss published the first formal solution, from a mathematical point of view, in 1809 [18]. But in the twentieth century, with the rise of space exploration, Lambert's problem interest renewed due to its importance for mission design applications, and so, many different approaches and contributions were made about the subject. However, in this thesis, the Lambert's problem will be approached using Roa's generalized logarithmic spirals [16], a shape-based approach.

5.1 Shape-based methods

This thesis will focus on low-thrust trajectory design, in other words, this thesis aims to solve the problem of a spacecraft accelerated by a continuous thrust that heads onto the asteroid belt. Low-thrust is a very powerful technique for the design of space missions, because it offers more possibilities than high-thrust and the high specific impulse of the propulsive systems improves greatly the accessibility and life operation time of the missions. Therefore, it has been the type of thrust chosen for this thesis due to its numerous advantages.

These low-thrust trajectories, as it was introduced in the previous chapters, have the particularity of developing slowly due to the low-thrust and thus degenerating in trajectories that spiral towards the central body. When facing a Lambert's problem of these characteristics, the first and maybe more obvious approach is to solve it as a optimal problem. But when put in practise, solving this optimal problem is often difficult, due to the wide range of possibilities it has, the initial guess choice and the convergence problems. Then some authors in the field searched for an analytic solution similar enough to the perturbed problem in order to reduce the computational cost inherent to the problem. Shape-based methods follow this line of work, they try to find trajectories that can be defined in closed form, to provide adequate initial guesses for more sophisticated optimization algorithms, but later studies showed the full potential of shape-based approaches, which can even constitute an excellent preliminary low-thrust trajectories design tool due to its capability for exploring large spaces of solutions.

Generalized logarithmic spirals method

There are many shape-based methods (for example the exponential sinusoid method, [19] and [20] and the finite Fourier series method [21]), but the generalized logarithmic spirals method was the one chosen for this thesis. The main advantage is that its solution is dynamically intuitive. Other methods introduce arbitrary parameters with no physic translation or intuitive meaning, but generalized logarithmic spirals parameters have a clear physical interpretation. For example, the constants K_1 and K_2, which defines completely the shape of the spirals, are the equivalent for the Keplerian energy and angular momentum. Therefore, working with these spirals is similar to working with Keplerian orbits and so, classical design techniques can be also applied to the low-thrust case. Also this facilitates the mission analysis in the design process.

5.2 Problem statement

A practical case of study will be presented in this section, a spacecraft leaving Earth headed to the asteroid belt. The belt is located between the orbits of Mars and Jupiter and it is estimated to harbor around 1.9 millions asteroids larger than 1 km in diameter and millions of smaller ones. Despite the enormous volume it occupies in space, the total mass of the asteroid belt is just 4% of the Moon mass, and half of it is concentrated in the four largest asteroids: Ceres, Vesta, Pallas and Hygiea. In a tribute to the Dawn mission and its recent discoveries about Ceres, obviously bridging the gaps, the objective asteroid of the mission of this thesis will also be Ceres.

Ceres is the largest asteroid in the belt. It is mainly composed of ice and rock. These are some of its orbit characteristics:

Semi-major axis: 414,010,000 km, about 2.7675 UA (note that the distance between the Sun and Earth is 1 UA).

Eccentricity : 0.075823 (because it is near 0, it will be considered to have a circular orbit).

Average orbital velocity: 17905 m/s

Assuming a circular orbit, the asteroid's angular velocity can be calculated as: $\omega_{ast} = v_{ast}/r_{ast}$ and so the position vector of the asteroid in each instant can be calculated:

$$\mathbf{r}(r, \theta, t) = (r_{ast}, \theta_{ast}(t), t) \quad \text{with} \quad \theta_{ast}(t) = \omega_{ast} * t + \theta_0$$

In order to reach the asteroid, the radius vector of the spacecraft has to coincide with the radius vector of the asteroid, this is: $\mathbf{r}_{spa}(r_{spa}, \theta_{spa}, t) = \mathbf{r}_{ast}(r_{ast}, \theta_{ast}, t)$. There are many spirals that enables this, intercepting the asteroid in different points, as figure 5.1 shows. It is interesting to note that the fastest spirals are hyperbolic spirals type I, whereas the rest of the spirals are elliptic spirals.

Usually, it is of more interest to specify the time when the spacecraft must reach the asteroid. This time is usually referred to as the time of flight, tof. Then, the problem reduces to find the spiral that connects Earth with Ceres in a specific time, so the condition to intercept the asteroid is now: $\mathbf{r}_{spa}(r_{spa}, \theta_{spa}, tof) = \mathbf{r}_{ast}(r_{ast}, \theta_{ast}, tof)$.

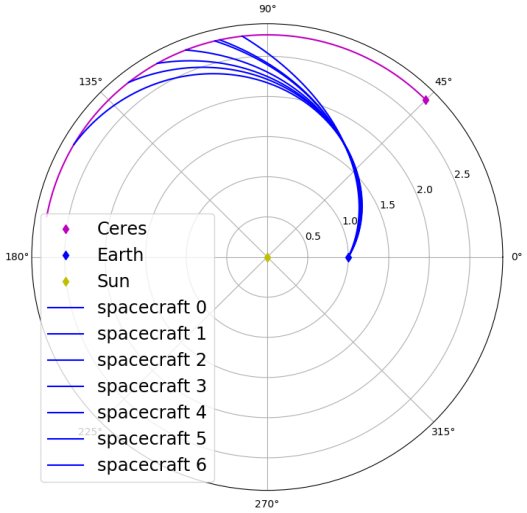

Figure 5.1: Seven different spirals that connect Earth's orbit with Ceres' orbit.

5.3 Solution approach

This section will describe the method followed in order to solve the spiral that connects a spacecraft leaving the Earth with the asteroid Ceres in the asteroid belt, in a specific time of flight, tof.

First, Earth and Ceres orbit data had to be known, so the way the planet and the asteroid moved and their relative position and distance could be implemented correctly. Recall that the assumption of Ceres having a circular orbit was taken. As it was said above, both radii r, angular position θ and time tof must match for the spacecraft and the asteroid. The problem is reduced to solve:

$$r_{ast} - r_{spa}(t) = 0$$

$$\theta_{ast}(t) - \theta_{spa}(t) = 0$$

$$t_{ast} - t_{spa} = 0$$

where $r_{spa}(t), \theta_{spa}(t)$ and t_{spa} can be obtained from the equations in chapter 3. Depending on the type of the spiral; r, θ and t will take different values until a spiral satisfies the three conditions from before. This system of equations will be solved numerically with the Python method from SciPy,

fsolve. To find the solution the code will iterate with the K_1 and K_2 values and with each iteration, it will initialize the spiral corresponding to those constants. Lastly, it will evaluate the system of equations until it is solved with a tolerance of $1e^{-12}$.

The method *fsolve* to be able to work needs at least three parameters: the function to solve, an initial guess of the solution and a tolerance value. The function was presented above as three equations and the tolerance value has been fixed to $1e^{-12}$. The critical point in this method is the initial guess, which for this problem is the spiral that best estimates the final solution. The initial guess is the difference between the method converging or not, so it is of vital importance.

The initial conditions are $r_0, v_0, \theta_0, \psi_0$ and t_0, where r_0 is the Earth orbital radius (1 AU), θ_0 is the angular position in the orbit around the Sun and t_0 is the moment of time in which the count starts. v_0 and ψ_0 depend on the launching of the spacecraft conditions. With all the initial conditions set, it is possible to calculate the K values of a spiral and so, completely define it (recall from equations 3.16 and 3.19 that with just r_0, v_0 and ψ_0 it is possible to completely define the shape of the spiral). Because r_0 is fixed by the launch place (Earth), the most critical values for obtaining a good initial guess are v_0 and ψ_0.

For isolated preliminary designs, by observing the relative position of the initial and final mission points it is possible to manually find the initial guess based on a priori estimated solution. But when trying to find an automatic initial guess finder, difficulty arises. This is because these type of spirals are very sensible to changes in their initial conditions, so little changes in them can translate into radical changes in the initial spirals guesses. This thesis did not find a consistent relation between the velocity of the launch v_0 and a good initial guess, but it did find a good relation for the parameter ψ_0. For large times of flight, the usual solutions are elliptic and parabolic spirals. Thus, parabolic spirals constitute in a way a limit for large times of flight. Therefore, solving for ψ in the parabolic equation of trajectory 3.39 yields:

$$\psi_1 = \arctan\left[\frac{\theta_2 - \theta_1}{\ln\left(r_2/r_1\right)}\right] \tag{5.1}$$

where 1 and 2 denote the start and end points respectively. Because this equation involves the distance and relative position between the start and end point, it yields good initial values of the parameter ψ_0. Effectively, when this equation was implemented on the code, the convergence rate greatly improved.

Figure 5.2 depicts the solution to the Lambert's problem for a $tof = 15$. The error, as the difference between the Earth and Ceres r, θ and t is of $4.44e^{-16}, 1.25e^{-11}$ and $4.47e^{-11}$ respectively, which is coherent for the tolerance imposed to the solver.

Note that, in the generalized logarithmic spirals equations, time was dimensionless. Earth spends one year in completing one revolution around the Sun, the equivalent in the spirals equations is a time of 2π. This yields a direct relation between the spirals time and the years time, for example in the case of figure 5.2 the time of flight was 15. The equivalent time measured in years is simply $15/2\pi = 2.39$ years.

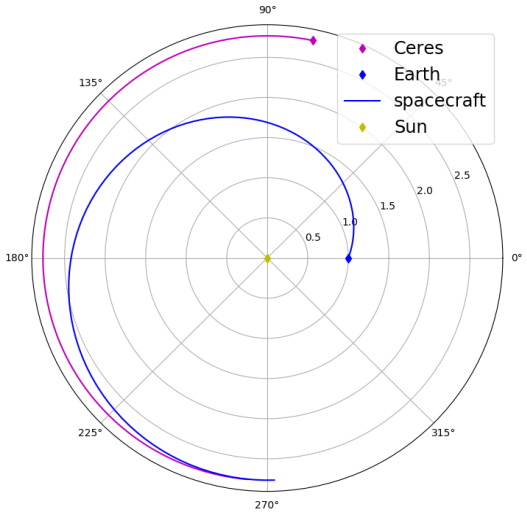

Figure 5.2: Connecting spiral between Earth and Ceres, for $tof = 15$.

5.4 Conclusions

The shape-based approach has proven useful when solving the Lambert's problem. The generalized logarithmic spirals method has reduced all the computation to solve a system of equations, which is way more simple than other method's computational requirements. Also, when analyzing the results, its physically intuitive characteristic makes easy to draw conclusions. For example, it was easy to see that large times of flight degenerate in elliptic spirals, which characteristics (i.e their negative Keplerian energy, or the existence of a maximum radius) are perfectly defined.

Chapter 6

Summary, Conclusions and Future Work

"Our virtues and our failings are inseparable, like force and matter. When they separate, man is no more."
-Nikola Tesla

6.1 Summary

The title of this thesis is *"Generalized Logarithmic Spirals for the Preliminary Design of Low-Thrust Trajectories to the Asteroid Belt"*. This thesis promised to study the low-thrust trajectories from the generalized logarithmic spirals shape-based approach in order to design a preliminary mission to the asteroid belt.

Indeed, this thesis has introduced and explained the most basic concepts of low-thrust trajectories, as well as the high-thrust trajectories, so advantages and disadvantages of each type of trajectory were displayed. This way, the choice of low-thrust trajectories has been justified.

In a similar way, the choice of the shape-based Lambert's problem approach over other methods, and more specifically the Generalized Logarithmic Spirals method choice, has been also justified by explaining its advantages over the others. This method has been deducted and developed accordingly, to later on implementing the method in a code, in order to use it in a practical trajectory design. The solution has been contrasted to ensure its validity.

The mission chosen was a trajectory to the asteroid Ceres, located in the asteroid belt.

6.2 Conclusions

The Generalized Logarithmic Spirals have proved the importance of the theory of regularization, which yielded this particular family of curves that this thesis has used. This solution has also proved to be valid and useful, mainly because of its clear physical interpretation of its constants and parameters. The Generalized Logarithmic Spirals have been implemented correctly, although some difficulties have been faced due to the complexity of the equations and structure of the solution. In exchange to these difficulties, once implemented properly, they have facilitated the preliminary design of the mission to the asteroid belt, reducing the complexity of the problem to little more that solving an equation system.

Overall, I agree with many others when saying that it is a very powerful method capable of exploring wide ranges of solutions with ease, making it perfect as an initial guess finder as well as a useful preliminary analysis mission tool.

6.3 Future Work

One interest future work line is to break down a spiral trajectory into smaller spiral trajectories. This way, instead of finding one single spiral that connect two points in space, one could have one trajectory composed by a number of spiral arcs. Each one would be chosen depending on the requirements of the mission phase at each section of the trajectory. This would result in a more optimal solution capable to adjust to the necessities of the mission at the different stages.

In order to do so and optimize each stage fuel for example, a control parameter for the thrust must be added to the Generalized Logarithmic Spirals model.

Lastly, in another future work line, one could approach the three dimensional Lambert's problem, instead of the two dimensional problem approached in this thesis.

List of Figures

List of Tables

Bibliography

[1] Smithsonian National Air and Space Museum. *NEAR Shoemaker*. URL: https://airandspace.si.edu/exhibitions/exploring-the-planets/online/solar-system/asteroids/exploration.cfm.

[2] NASA. *Dawn Mission Overview*. URL: https://dawn.jpl.nasa.gov/mission/.

[3] NASA. *OSIRIS-REx*. Aug. 2017. URL: https://www.asteroidmission.org/mission/.

[4] NASA. *NEAR Shoemaker*. Aug. 2017. URL: https://www.nasa.gov/content/goddard/lucy-the-first-mission-to-jupiter-s-trojans.

[5] Southwest Research Institute. *Lucy's orbital path*. Aug. 2017. URL: https://www.nasa.gov/sites/default/files/thumbnails/image/ta010359_lucy3-b-orbit-crop.png.

[6] NASA. *NASA FY 2018 BUDGET REQUEST*. May 2017. URL: https://www.nasa.gov/sites/default/files/atoms/files/fy_2018_agency_fact_sheet.pdf.

[7] *NASA budget comparison*. Sept. 2014. URL: https://en.wikipedia.org/wiki/Budget_of_NASA.

[8] Michael Sheetz. *Number of VC's investing in space*. Jan. 2018. URL: https://www.cnbc.com/2018/01/18/space-companies-got-3-point-9-billion-in-venture-capital-last-year-report.html.

[9] Planetary Resources CEO Chris Lewicki. *Article about Arkyd-6*. Apr. 2018. URL: https://www.planetaryresources.com/2018/04/mission-success-arkyd-6-tests-key-technologies-for-commercial-space-resource-exploration/.

[10] Howard D.Curtis. *Orbital Mechanics for Engineering Students*. 3rd ed. Dec. 2004. Chap. 6.

[11] NASA. *Ion Propulsion*. Aug. 2017. URL: https://www.nasa.gov/centers/glenn/about/fs21grc.html.

[12] ESA. *Solar Sails*. URL: http://www.esa.int/Education/Solar_sails.

[13] NASA. *Electromagnetic Propulsion Systems*.

[14] "Pathways to Mars" by John C. Niehoff and Stephen J. Hoffman. *Table comparing the specific impulse of different types of rockets*. Mar. 2015. URL: http://web.archive.org/web/20050205102227/http://marsacademy.com:80/propul/propul3.htm.

[15] Howard D.Curtis. *Orbital Mechanics for Engineering Students*. 3rd ed. Dec. 2004. 768 pp.

[16] Javier Roa Vicens. "Regularization in Astrodynamics: applications to relative motion, low-thrust missions, and orbit propagation". PhD thesis. Universidad Politecnica de Madrid, Sept. 2016.

[17] R.H. Bacon. "Logarithmic spiral: An ideal trajectory for the interplanetary vehicle with engines of low sustained thrust". In: (1959), pp. 164–165.

[18] C.F. Gauss. *Theoria motus corporum coelestium in sectionibus conicis solem ambientium*. 1809.

[19] Anastassios Evangelos Petropoulos. "A shape-based approach to automated, low-thrust, gravity-assist trajectory design". PhD thesis. Purdue University, 2001.

[20] Anastassios E. Petropoulos and James M. Longuski. "Shape-Based Algorithm for the Automated Design of Low-Thrust, Gravity Assist Trajectories". In: *Journal of Spacecraft and Rockets* (Sept. 2004), pp. 787–796.

[21] Chong Sun Qun Fang Xuefeng Wang and Jianping Yuan. *A Shape-Based Method for Continuous Low-Thrust Trajectory Design between Circular Coplanar Orbits*. Apr. 2017.